Chapter 5

How Bright is the Coast of Brittany?

Shaun Lovejoy[*] *and Daniel Schertzer*[†]

1 Introduction

1.1 Fractal sets and multifractal measures

As long ago as 1913, Jean Perrin noted that the usual notions of measurement were perhaps not adequate for answering the seemingly simple question 'How long is the coast of Brittany?'[1], and Steinhaus (1954) noted that rivers were 'not rectifiable'[2]. It wasn't until many decades later that a clear answer became at all accepted. It now seems obvious that there is 'something' fractal about a coastline, hence today, even laymen understand that the length depends fundamentally on the resolution at which it is measured.

If there is no unique (scale independent) length of a coastline, then why should their be a unique fractional cloud cover (forest cover) etc? Indeed, over the last decade, it has been noticed that as the resolution of satellites improves, the estimates of global albedo are consistently declining. Estimates of fractional cloud cover are also known to decline -sometimes

[*]Physics Department, McGill University, Montréal, Canada

[†]Laboratoire de Météorologie Dynamique, Université Pierre et Marie Curie, Paris

[1]Mandelbrot, 1967, building on Richardson's 1961 scaling analyses suggested that a fractal dimension was the appropriate characterization of the scaling

[2]'...the left bank of the Vistula, when measured with increased precision woud furnish lengths ten, hundred and even thousand times as great as the length read off a school map. A statement nearly adequate to reality would be to call most arcs encountered in nature as not rectifiable. This statement is contrary to the belief that not rectifiable arcs are an invention of the mathematicians and that natural arcs are rectifiable: it is the opposite that is true...' Steinhaus, 1954. To prove his point, Steinhaus 1962 shows a (fractal) Peano curve

precipitously- with improved resolution. Indeed, Gabriel et al. 1988, have shown that the effect is systematic no matter what brightness thresholds are used to estimate the cloud fraction[3]. Similarly, the resolution dependence of the coastline has now been generalized to all topographic level sets (not just sea level); Lovejoy and Schertzer 1990 have shown the same effect on regions exceeding various altitudes on the earth. How is it therefore that the analogous conclusion - now obvious for coastlines - has not been drawn for remotely sensed radiances? A partial answer to this question may be that remote sensing deals with measures and their integrals over various resolutions ('pixel elements'), not with geometric points of sets (such as the borderline between zones above and below sea level). While the framework necessary for dealing with the latter has been around for quite some time (see especially Mandelbrot 1983), the corresponding multifractal framework necessary for dealing with measures and fields, is little over ten years old (1983). In the following, we argue that there is now ample theoretical and empirical evidence for recognizing this resolution dependency as a basic aspect of remote sensing. Its implications must be fully pursued in the development of resolution independent remote sensing algorithms.

This chapter will review a small part of what is a mushrooming field, aiming to give a brief synopsis of different aspects of a large body of work. Several more pedagogical introductions to multifractals are now available, see especially Schertzer and Lovejoy 1994a. In a companion paper (Schertzer and Lovejoy 1994b, hereafter labeled SL94), we concentrate on more recent advances in multifractals and how they can be used in remote sensing.

1.2 Clouds

Before considering multifractals and multifractal analyses (which involve an exponent function rather than a unïque exponent values), we will give some examples of the scaling of some basic geophysical fields (clouds, wind and Earth's surface) using standard energy spectra ($E(k)$ for the energy at wavenumber k). Scale invariance implies invariance under 'zooms', the simplest of which is the isotropic zoom $\underline{x} \rightarrow \lambda \underline{x}$ (see section 4 for generalizations), hence $\underline{k} \rightarrow \lambda^{-1} \underline{k}$. Invariance will be associated with power laws:

$$E(k) \approx k^{-\beta} \tag{1}$$

[3]They even used statistical hypothesis testing to show that resolution independent cloud brightness fractions did not exist for any significant brightness levels

since only power laws retain their form under zooms (in section 4, we shall see that more precisely, they have the required group properties). We shall see that the spectral exponent β is related to a single value of the moment function $K(q)$ (defined in section 2): $\beta = 1 - K(2)$ (the value 2 because spectra are second order statistics).

There has long been uncertainty over the exact type and range of scaling in the atmosphere. Since the 1950's the basic model postulated isotropic two dimensional turbulence at large scales, and isotropic three dimensional turbulence at large scales, the two being seperated by a hypothetical 'meso-scale' gap or 'dimensional transition' (supposedly at about 10km, the scale height of the mean pressure). The recognition of scale invariance as a basic dynamical symmetry principle ('Generalized Scale Invariance', Schertzer and Lovejoy 1985a,b) in the 1980's made the standard model seem quite ad hoc since it was much simpler to postulate scaling, but without the restriction to isotropy. The resulting 'unified scaling model' (Lovejoy et al. 1993, Chiriginskaya et al. 1994, Lazarev et al. 1994) seems to be very close to the measurements (see fig. 1 for a schematic diagram). Indeed, figs. 2, 3 show some recent aircraft and radiosonde spectra indicating that through the entire atmosphere in the vertical (and right through the meso-scale in the horizontal), that the scaling is well obeyed, although the exponents are quite different in the two directions (defining an 'elliptical dimension'$\approx$ 23/9, see section 4).

In order to clarify the situation in the horizontal, (specifically to augment the number of samples of large structures so as to obtain good statistics) satellite radiances are analyzed in fig. 4 with no evidence of a break in the horizontal scaling over at least the range $\approx$ 300m to $\approx$ 4000km. Since the cloud radiances are nonlinearly coupled with the dynamics, the absence of a break in the radiances will reflect the absence of a break in the dynamics. To extend this range to smaller scales, figs. 5, 6 show that the corresponding cloud liquid water content is scaling over at least the range $\approx$ 5m to $\approx$ 330km. Recent results on rain (Lovejoy and Schertzer 1990) extend the latter limit down to millimeter scales and it has long been known that atmospheric turbulence is scaling from dissipation scales of less than millimeters to much larger scales. These findings (combined with many others, see Lovejoy et al. 1993 for a review) make it likely that the atmosphere is scaling over the entire meteorologically significant range.

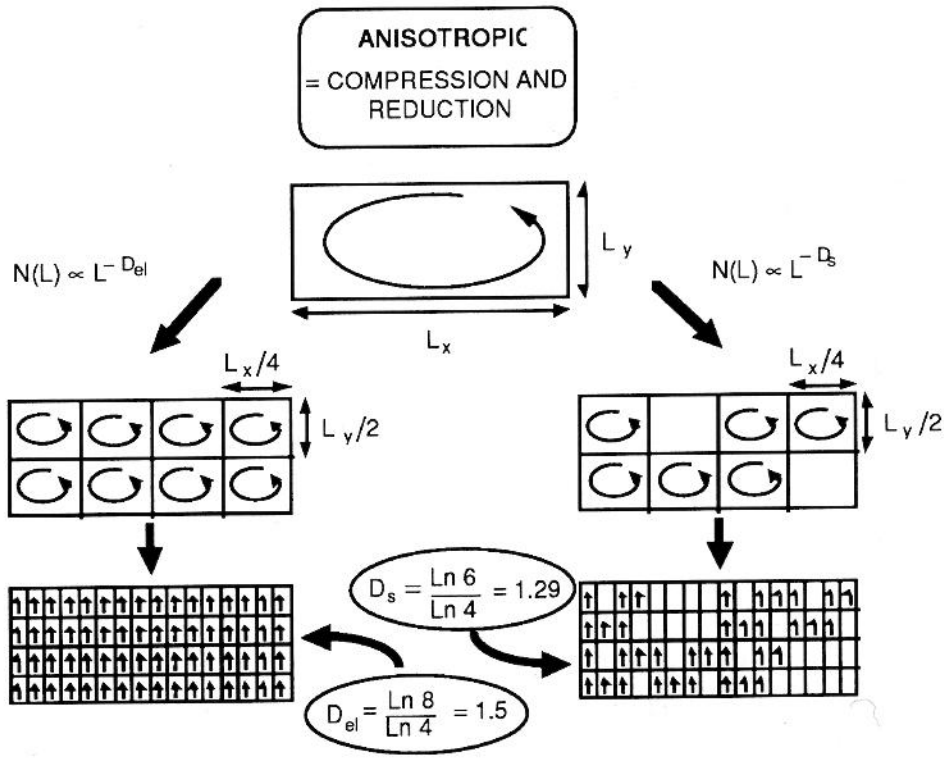

Figure 1: Anisotropic cascade scheme showing how the vertical cross-section of a large (horizontally flattened eddy) gets broken into s. aller sub-eddies in a scaling anisotropic manner. The elliptical dimension used here is 3/2 (from Lovejoy and Schertzer 1986.)

1.3 Surfaces

The other field fundamental for remote sensing is the Earth's surface. It has long been known (Venig-Meiniz, 1951) that the topography has a power law spectrum over wide ranges. However, during the 1980's the scaling properties and limits were somewhat obscured when attempts were made using inappropriate monofractal analysis techniques to fit the multifractal topography (see below) into monofractal frameworks. For example, debates arose around which was the most appropriate value of the supposedly unique fractal dimension of altitude isolines. Research has shown that there is no unique value; the fractal dimension systematically decreases for higher and higher altitude thresholds. This implies that the monofractal frame-

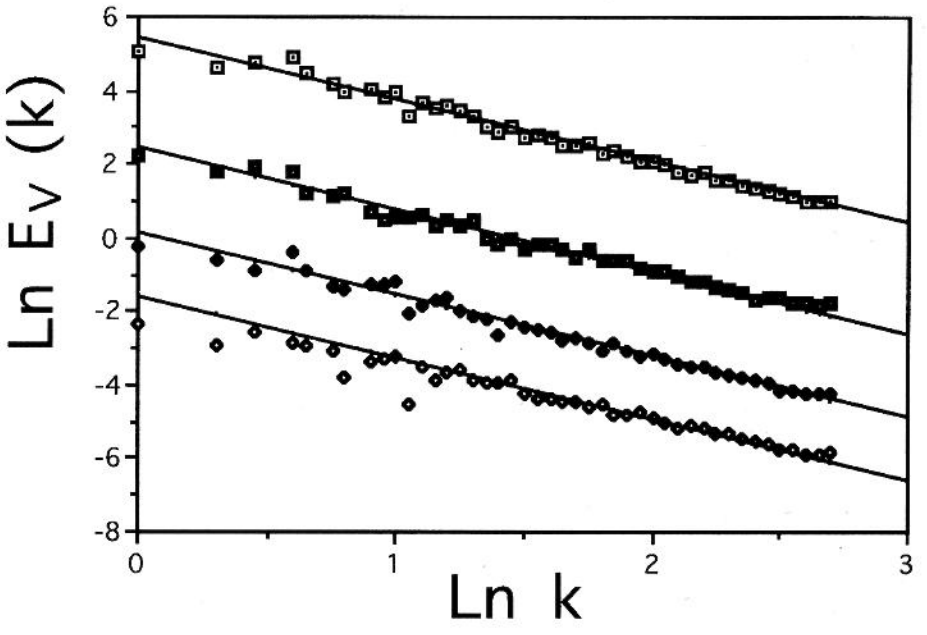

Figure 2: The spectrum of temperature fluctuations. Top: average over the 3 air craft data sets taken roughly at one year interval in the tropics (each contains 10 samples). Below: 3 individual spectra obtained by averaging over the 10 samples. The absolute slopes are close to Corssin-Obukhov value 5/3: $\beta_v = 1.68 \pm 0.05$ over the frequencies range $\omega_0/20 - \omega_0/20480(\omega_0 = 8\text{Hz})$. From Chiriginskaya et al. 1994.

work of self-affine surfaces (which cannot handle multiple dimensions) is inappropriate.

When surfaces are remotely sensed, there is usually no simple or direct relation between the physical surface or atmospheric parameters and the observed radiances. Below we will argue with examples, that serious exploitation of remotely sensed data requires the use of multifractal models of the radiation/matter interactions. For the moment, we consider another example: ice surfaces observed by airborne Synthetic Aperture Radar (SAR); fig. 7 shows the result at different wavelengths and polarizations. Full treatment of these correlated multifractals requires (complex) Lie cascades (see section 5, the accompanying text, and Schertzer and Lovejoy 1994).

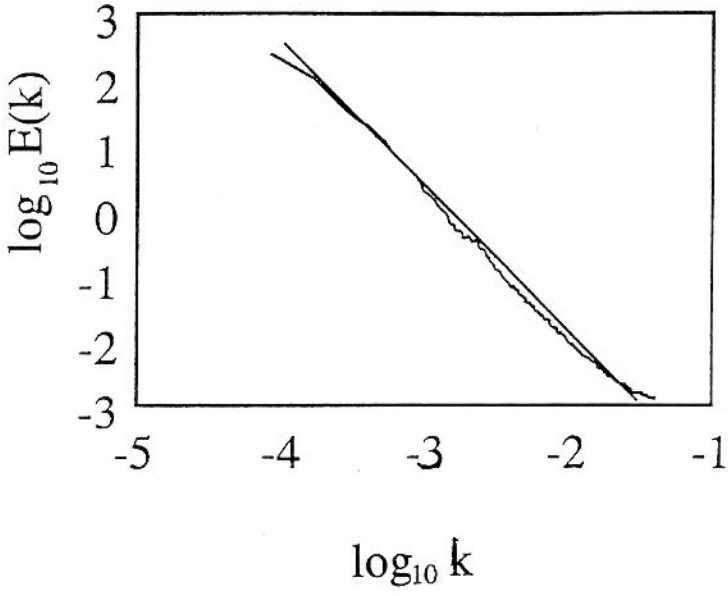

Figure 3: The mean spectrum of 280 radiosondes at 50m resolution, over a total depth of 13.3km, taken in the tropics (same experiment as fig. 2). The straight line is the theoretical line (Bogliano-Obhukhov scaling) with $H_v = 3/5; \beta_v = 2.20$. The scaling is well respected throughout the entire thickness of the atmosphere.

2 Properties of Multifractals

2.1 Discussion

The full implications of nonlinear dynamics coupled with scaling have only begun to be grasped in the last few years. It is now increasingly clear that this generally leads to multifractal behaviour (see e.g. Schertzer and Lovejoy 1991). Multifractals have highly singular small scale limits; they do not converge in the sense of functions, but only weakly, in the sense of measures. Although at first sight this may seem to be an academic distinction, it is in fact fundamental. When multifractal fields are measured by remote or in situ sensors whose temporal or spatial resolution is much lower than that of the intrinsic variability of the phenomenon (which can easily be of the order of millimeters and milliseconds), then the result is a low resolution function whose properties depend fundamentally (in precise

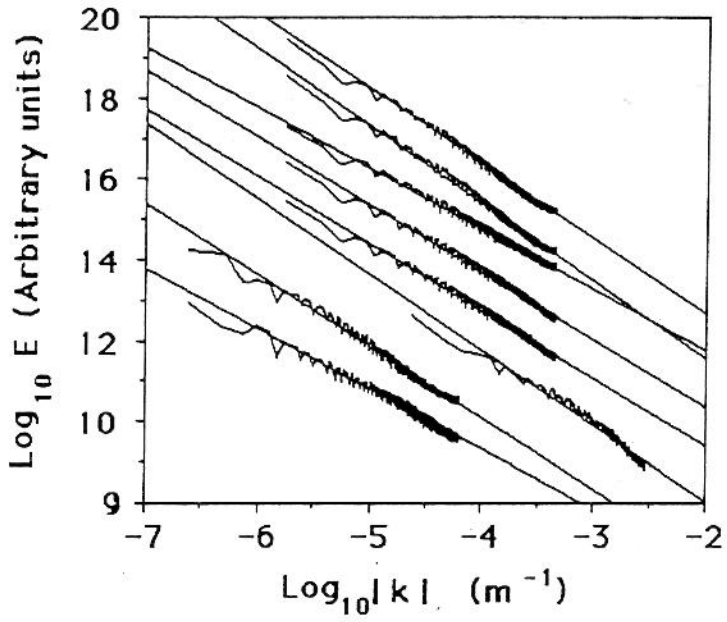

Figure 4: Average power spectrum for satellite images grouped according to the satellite and the frequency range of the images (from bottom to top): LANDSAT (visible) $\beta = 1.7$, GOES (visible) $\beta = 1.4$, GOES (infra-red) $\beta = 1.7$, Nimbus-9 (channel 1 to 5) $\beta = 1.67, 1.67, 1.49, 1.91, 1.85$. (See Tessier et al. 1993b, Lovejoy et al. 1993).

power law ways) on the resolution.

Denote the ratio of the largest (e.g. satellite image) scale by L, and the smallest (e.g. single pixel) scale by l, and the ratio $\frac{L}{l} = \lambda(> 1)$. We can then denote the field of interest (e.g. satellite radiance) at resolution l by ε_λ which will have the following 'multiscaling' behaviour (Schertzer and Lovejoy 1987):

$$Pr(\varepsilon_\lambda \geq \lambda^\gamma) \approx \lambda^{-c(\gamma)} \tag{2}$$

where Pr indicates 'probability', γ is the 'order of singularity' associated with the threshold value ε_λ, and $c(\gamma) \geq 0$ is the corresponding 'codimension'. As the resolution (γ) is increased, the satellite will see more and more small bright regions; for a scale invariant field, γ is the correct way to remove the systematic resolution dependencies. Similarly, $c(\gamma)$ indicates how the histograms of brightness values will change with resolution, and provides the appropriate way of removing the scale dependence of the his-

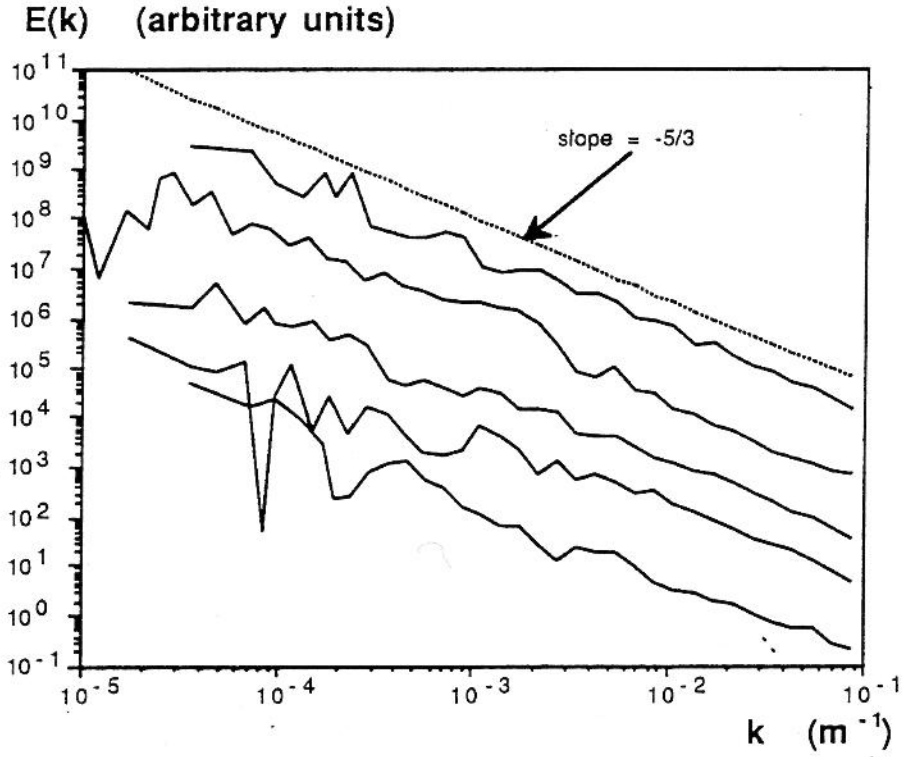

Figure 5: Power spectrum of 5 different aircraft liquid water concentration data sets (averaged to 10 points per magnitude on the k-axis, resolution $\approx$ 5m). All the sets are very well scaling and have absolute slopes close to the theoretical value for passive scalars $\beta = \frac{5}{3}$ (straight line on top of graph). In order to avoid overlapping of the different curves, the lines were offset vertically. Number of data sets from top to bottom with vertical offset given in brackets: 4 (10^5), 3 (10^4), 1 (10^2), 2 (10^1), 5. From Brosamlen et al. 1994.

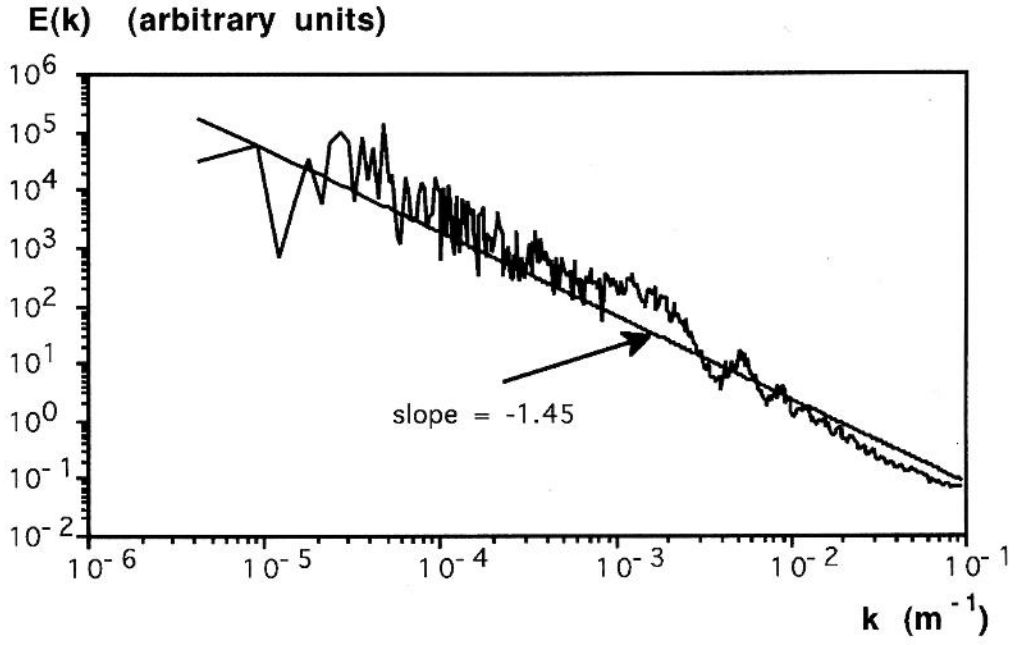

Figure 6: Aircraft liquid water concentration data sets power spectrum (averaged to 100 points per magnitude on the k axis. This shows a remarkably good scaling right through the meso-scale ($\approx$ 10km, the graph covers the range of $\approx$ 10m to $\approx$ 300km). From Brosamlen et al. 1994.

tograms. The behaviour indicated in eq. 2 will of course break down for large enough λ (small enough l, often of the order of millimeters), but over its range of validity, it represents a very strong effect since ε_λ and the probabilities will respectively diverge and converge as λ increases. When, $c(\gamma) < D$ (D being the dimension of the observing space; =2 for images) $c(\gamma)$ is the (geometrical) codimension $c(\gamma) = D - D(\gamma)$ corresponding to the (geometrical) fractal dimension $D(\gamma)$ of the support of singularities whose order is greater than γ. The basic physical model for such behaviour are cascade processes in which the large scale multiplicatively modulates the smaller scales, in a mechanism that repeats from one scale to another over a very large range. Note that for the moment, we consider only isotropic scale changes associated with self-similar multifractals, full treatment of geophysical fields requires Generalised Scale Invariance (GSI, Schertzer and Lovejoy 1985a,b, 1989, 1991) which involves anisotropic scale changes and

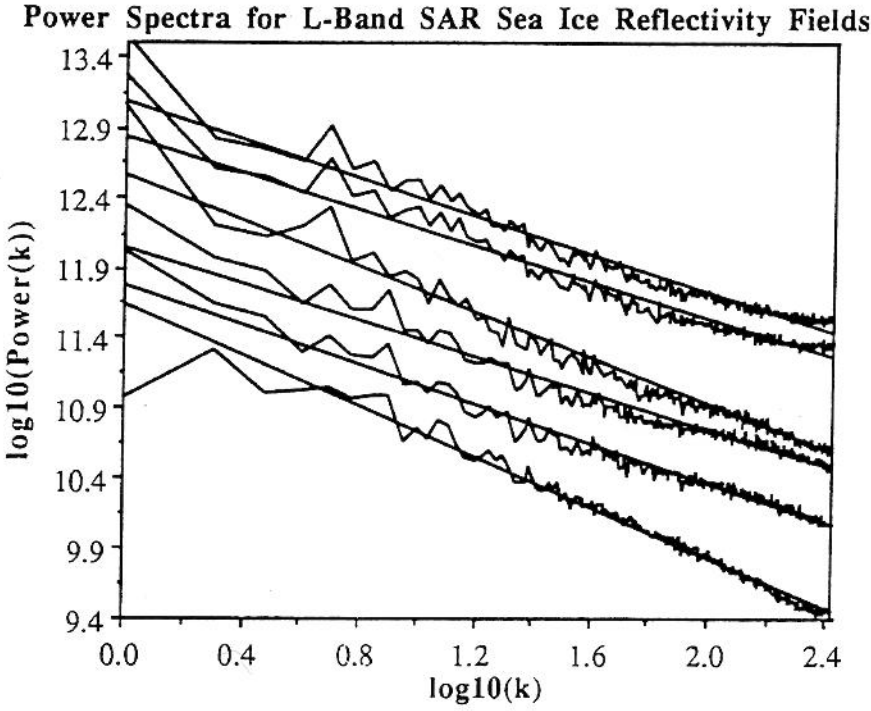

Figure 7: Power spectra of synthetic aperture radar data of two scenes (512 x 512 points each) of sea ice at 12.5m resolution showing that the scaling is well respected, especially in the HV polarization in both the SAR C-band data scenes (from top to bottom, the curves are HH, VV and HV for scene 1 and HH, VV and HV for scene 2 respectively. They were offset by 0.5 in the vertical so as to not overlap. From Francis et al. 1994.

is necessary to account for the 'texture' and 'morphology' of structures (see e.g. Pflug et al. 1993 for a recent study of cloud texture and type and section 4).

The multiple scaling behaviour of this field ε at scale ratio λ ($=\frac{L}{l}$ the ratio of the largest scale L to the scale l) can be also be characterized by the corresponding law for the statistical moments (via a Laplace transform):

$$\lambda^{K(q)} = \langle \varepsilon_\lambda^q \rangle = \int \lambda^{q\gamma\lambda - c(\gamma)} d\gamma \qquad (3)$$

(the symbol '$\langle . \rangle$' indicates statistical averaging). All satellite and radar measurements of the atmosphere or surface which obey eq.s 2, 3 are strongly dependent on the characteristics of the sensor (via the ratio γ); they are

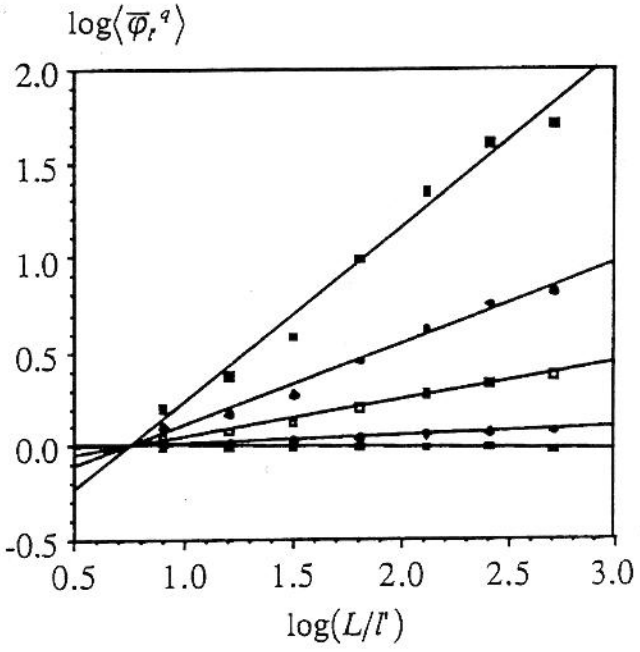

Figure 8: The scaling behaviour of the statistical moments of the Deadman's Butte data is illustrated here by the straightness of the curves of the $\log\langle\bar{\phi}_l^q\rangle$ as functions of $\log(L/l)$, with L the largest scale in the Digital Elevation Model: from bottom to top $q = 0.5$, 1.5, 2.5, 3.5 and 5. The slopes correspond to the scaling exponent $K(q)$. From Lovejoy et al. 1994c.

not pure functions of the state of the atmosphere or surface that we are measuring. Since detailed comparisons of remote measurements at different resolutions are seldom made, workers in the field are only just starting to realize the importance of these resolution effects. What we propose is the systematic development of new resolution-independent algorithms for calibrating and exploiting remotely sensed data. This will also involve a systematic characterization of the types and limits of scaling of the various fields.

Some examples of multiscaling of the moments are shown in fig. 8 which shows the scaling of the moments of the quantity ϕ (the quantity correspoding to ε) for the topography at Deadman's Butte, and fig. 9 shows the corresponding $K(q)$ function. Monofractal topographies (such as those of the celebrated monofractal landscapes illustrating Mandelbrot's book), would be linear. Below, we indicate how to quantify this degree of

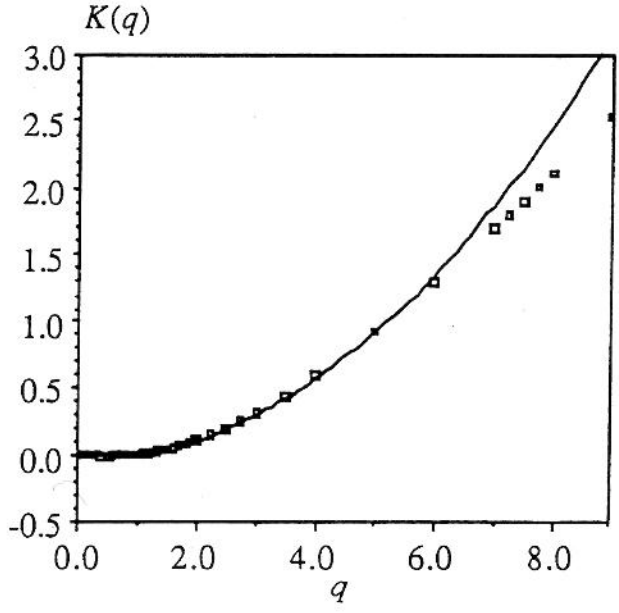

Figure 9: The scaling exponent $K(q)$ against q for the Deadman's Butte data (see figs. 8). The continuous curve is the theoretical universal multifractal fit with $\alpha = 1.9$, $C_1 = 0.05$ (see eq. 9) For $q > 6$, the asymptotic behavior of $K(q)$ becomes linear. This is a second order multifractal phase transition predicted from the finite sample size. From Lovejoy et al. 1994c.

multifractality more precisely with the help of universal multifractals.

2.2 A few properties

In general, knowledge of the probability distributions is equivalent to knowledge of all the statistical moments of a process; in multifractals, this relationship is particularly simple. In eq. 3, only the maximum exponent dominates in the integral, and the (Laplace) transform relating the moments and probabilites reduces to a Legendre transform for the exponents (Parisi and Frisch 1985).

$$K(q) = max_\gamma(q\gamma - c(\gamma)) \;\; c(\gamma) = max_q(q\gamma - K(q)) \tag{4}$$

These relations establish a one to one correspondence between orders of singularities and moments ($q = c'(\gamma), \gamma = K'(q)$). Both the codimension function $c(\gamma)$ and the moment scaling exponent $K(q)$ are convex. Note that in practice, the maximum order of singularity available in a sample is bounded simply due to the finite sample size; the resulting restrictions on the γ in the above maximization, are associated with multifractal phase transitions as discussed in SL94.

Various types of multifractals exist; and they can profitably be classified according to their highest order of singularity (see Schertzer et al. 1991, and Schertzer and Lovejoy 1992). Unfortunately, those which have been most extensively studied; the geometric multifractals in strange attractors, or the microcanonical multifractals often used as a framework for analysing turbulence (e.g. the celebrated 'p model', Meneveau and Sreenivasan, 1987), are artificially restricted so that high order singularities cannot occur. In contrast, the general 'canonical' multifractals generically produced by cascade processes do not suffer from these restrictions. In canonical multifractals, the existence of occasional 'hard' (very violent) singularities leads to quite different behaviour for the (theoretical) process without the small scale interactions ('bare' properties), and for the same process with the small scale interactions ('dressed' properties). The latter are the result for example when cascade processes proceed down to infinitely small scales and are then integrated over finite scales (for example by a remote sensor). The dressed ε_λ, will generally display the phenomenon of divergence of high order statisitical moments, and are discussed in more detail in SL94.

2.3 Universal multifactals

One of the most fruitful physical ideas is that of universality; that of all the complex details of a process, that -if it is repeated sufficiently often for example over a wide enough range of scales - that only a few of the details will actually matter. Each resulting 'universality class' has a basin of attraction which determined by all the set of parameters which give the same limiting behaviour. In multiplicative process and multifractals, the question of universality has a long history, much of it being connected with the 'law of proportional effect' and lognormal distributions. Unfortunately, for various technical reasons (discussed in more detail in SL94), for several years, an anti-universality prejudice developed in the multifractal literature. The absence of universality would have dire implications for the very possibility of using multifractals for anything since it would mean that an infinite number of theoretical parameters would be needed to specify every multifractal process (e.g. the entire $c(\gamma)$ or $K(q)$ function). Similarly, the corresponding empirical characterization would also be impossible. Fortunately, stable, attractive universality classes do exist for multifractal processes, a fact that is being increasingly recognized (Schertzer and Lovejoy 1987, 1989, Fan 1989, Brax and Peschansky 1991, Kida 1991, Dremin 1994 etc.).

Multiplying processes corresponds to adding generators. We seek *generators* which are *stable* and *attractive* under *addition*. Considering for the moment only stationary (conservative) multifractals, these generators yield the *universal* expressions (Schertzer and Lovejoy 1987, 1989) for the scaling function of the moments of the field $K(q)$ and of the codimension function $c(\gamma)$:

$$c(\gamma) = C_1 \left(\frac{\gamma}{C_1 \alpha'} + \frac{1}{\alpha} \right) \alpha' \quad \alpha \neq 1 \tag{5}$$

$$K(q) = \frac{C_1}{\alpha - 1} (q^\alpha - q) \quad \alpha \neq 1 \tag{6}$$

where $(\frac{1}{\alpha} + \frac{1}{\alpha'}) = 1$, and when $\alpha < 2$, for $q = c'(\gamma) > 0$. α is the Levy index of the generator and characterizes the degree of multifractality. The $\alpha = 2$ case corresponds to the maximal degree of multifractality and the bare $\alpha = 2$ multifractal has lognormal probabilities. The $\alpha = 0$ case corresponds to the monofractal minimum. C_1 is the codimension of the mean and characterizes the sparseness of the mean field. H is the degree of nonconservation and characterizes the degree of nonstationarity of the process. Note that the lognormal multifractals are compatible with the lognormal phenomenology of geophysics.

2.4 The degree of non-stationarity: the Hurst exponent H

Most fields observed in nature are not conserved, i.e. the average of the observed quantity at scale λ (denoted here by:$\langle\rho_\lambda\rangle$) is not equal at different scales. This requires the introduction of a third[4] universal multifractal parameter H (the 'Hurst' exponent) which measures the degree of nonstationarity in the process; it is also a measure of the conservation of the field over different scales (as the casc ade proceeds to smaller scales), e.g. $H = 0$ is a conserved or stationary multifractal[5]. For many analysis techniques it is necessary to isolate the underlying conserved quantity (see below).

To understand this better, consider the relatively well studied case of passive scalar advection. If cloud droplets were passive scalars, i.e. transported by the wind without interacting with it, one obtains the Corrsin-Obhukhov law for passive scalars (Obhukhov 1949, Corrsin 1951):

$$\Delta\rho_\lambda = \phi_\lambda^{\frac{1}{3}}\lambda^{-\frac{1}{3}} \tag{7}$$

$$\phi_\lambda = \chi_\lambda^{\frac{3}{2}}\varepsilon_\lambda^{-\frac{1}{2}} \tag{8}$$

where ε_λ is the turbulent energy flux and χ_λ is the passive scalar variance flux[6] at scale ratio λ. Eq. 7 indicates that $H = 1/3$. $\Delta\rho_\lambda = \rho(x + \lambda^{-1}L) - \rho(x)$ is the density fluctuation at scale λ. Without intermittency, χ_λ and ε_λ are constants (have trivial scale dependency) with (scaling) intermittency then χ_λ and ε_λ will be multifractal and ϕ_λ will obey eqs. 2, 3. More generally, since liquid water is not really passive (for example it is associated with latent heat release which modifies the velocity field) we may still consider that the characteristic fluctuations $\Delta\rho_\lambda$ are scale invariant and write the scaling for the density ρ as:

$$|\Delta\rho|_\lambda \approx \phi_\lambda^\alpha\lambda^{-H} \tag{9}$$

[4]Davis et al. 1994 have proposed characterizing multifractals with just *two* parameters (C_1, H); these are clearly only sufficient to determine the tangent of $K(q)$ near q=1, i.e. the best *mono* fractal approximation. To discuss any *multi* fractal characterization, at least three parameters are necessary, α is the natural choice

[5]If $H > 0$ the process is nonstationary i.e. it is statistically translationally invariant. A more restricted notion of stationarity (second order stationarity) depends on the value of β (a process is second order stationary if $\beta < 1$). The distinctions between true stationarity (discussed here) and second order stationarity (which has no special significance for multifractals) have sometimes been forgotten (e.g. Davis et al. 1994)

[6]Note that as indicated Corssin-Obhukov scaling involves quasi steady fluxes; these boundary conditions are totally different from those of point dispersion pollutants

where ϕ_λ has the conserved property $\langle \phi_\lambda \rangle = constant$ (independent of scale). Since we have as yet no proper dynamical theory for the liquid-water distribution in the atmosphere, we do not know the appropriate fields ϕ_λ nor the corresponding value of a. However, changing the value of a corresponds essentially to changing the parameter C_1, (Schertzer and Lovejoy 1994), without loss of generality, we therefore set it equal to 1.

3 Multifractal analysis and simulation techniques

3.1 Summary of multifractal data analyses

Table 1 summarizes some recent studies of universal multifractal characteristics of various fields, many of them remotely sensed. Most of these estimates were obtained using the Double Trace Moment (DTM) technique (Lavallé 1991). This method is based a generalization of the above obtained by first raising the field at the smallest available resolution (indicated by Λ) to the power η, then degrading to resolution λ before averaging over the qth power of the result:

$$\langle (\varepsilon_\Lambda^\eta)_\lambda^q \rangle = \lambda^{K(q,\eta)} \tag{10}$$

Since we are considering the normalized η powers, the q, η scaling exponent function is related to the usual exponent by:

$$K(q,\eta) = K(q\eta) - qK(\eta) \tag{11}$$

The usefulness of the double trace moment technique becomes apparent when it is applied to universal multifractals since in this case, we have the following:

$$K(q,\eta) \backsimeq \eta^\alpha K(q,1) \tag{12}$$

i.e. $\log K$ vs. $\log \eta$ will be linear over the region where the above holds. Since eq. 12 is strictly true only for bare moments, the finite sample and/or divergence of moments will cause it to break down for large q, η (q or $q\eta > q_S$). At small η, it can also break down due to the presence of noise or zero values. Figs. 10, 11, 12 give some examples on surfaces.

Table 1 contains a more complete list including universality parameters, sampling limits, critical orders and singularities of divergence (corresponding to 'hard' multifractals and Self-Organized Critical structures; see SL94), as well as the effective dimension of dressing (see SL94 for more details).

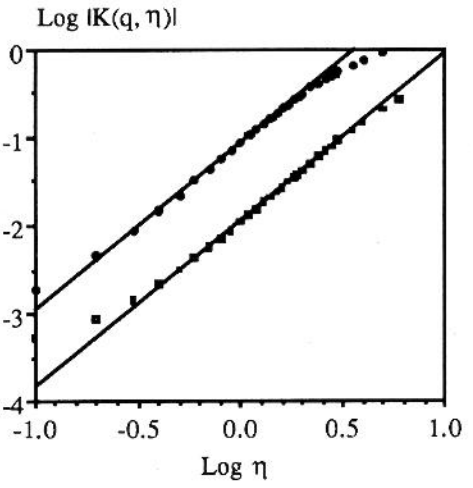

Figure 10: The curves of $\log|K(q,\eta)|$ as functions of $\log\eta$, for the Deadman's Butte data. From top to bottom q takes the values 2 and 0.5. All the curves are parallel as predicted by universality eq. 12. The evaluation of their slopes, with η taking values between en 0.5 and 2.4, gives the following values of α : 1.90 ± 0.1 and 1.89 ± 0.1. The values of C_1, obtained by solving the expression for $\log\eta = 0$ intercept given by $\log|K(h,l)|$ and using eq. (12), are respectively: 0.044 ± 0.05 and 0.045 ± 0.05. The consistency between the estimates of α, C_1 for various values of q, are good indications that they are accurate. For values of η too high or too low, the curve $K(q,\eta)$ becomes (fairly) constant, and these values of $\log|K(q,\eta)|$ must not be considered to estimate α. From Lavallée et al. 1993.

Two aspects are worth noting. First, almost all of the α values are > 1, hence the corresponding processes are 'unconditionally hard', i.e. for any finite D, a finite q_D exists; some moments will diverge. Self-organized criticality therefore seems to be prevalent and γ_D gives a quantitative measure of the intensities of the self-organized critical strucutres. Second, we see that C_1 is often smaller than H (see. e.g. topography or turbulence), hence the multifractality - while being nearly maximal according to the observed value of α - will nevertheless not be too pronounced unless we consider the extreme events; monofractal models can therefore

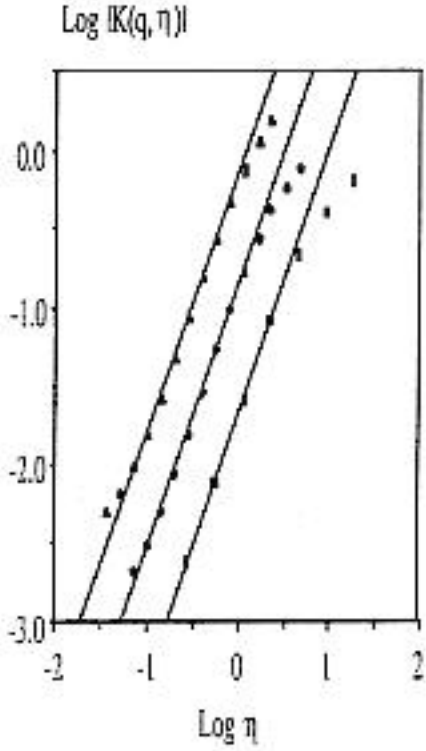

Figure 11: Same as fig. 10 but for the French topography at 1km resolution. From top to bottom q takes the following values: 4, 2 and 0.5. All the curves are parallel as predicted by eq. (12). The estimates of the slope for $q = 4$, with η taking values between 0.1 and 0.5, gives $\alpha = 1.67 \pm 0.1$. The same analysis for $q = 2$ and 0.5 (with η taking values between 0.12 and 1.1 in the first case and between 0.3 and 2.3 in the second), yield respectively $\alpha = 1.69 \pm 0.1$ and 1.7 ± 0.1. The values of C_1, obtained by solving the expression for the $\log \eta = 0$ intercept given by $\log |K(q, l)|$ and using eq. 12, are respectively: 0.078 ± 0.05, 0.076 ± 0.05 and 0.076 ± 0.05. Here also the values of α, C_1 determined are independent of the q values. From Lavallée et al. 1993.

ld	Type	α	C_1	H	q_D	q_s[c2]	γ_D	D	Range of scales
on ds	Clouds, Visible, Infra red[a]	1.35	0.15	0.3-0.4[b]	>5	6.8	—	—	160m→ 4000km
	Clouds Microwave[b1]	1.35	0.10	0.3-0.5[b]	—	9.2	—	—	10km→ 2000km
	Rain Radar reflectivity[c]	1.35	0.30	0.0	1.1-2[d]	4.1	0.6-0.8	0.4-0.5	30m→ 64km
	Rain Raingauge, horizontal[c]	1.35	0.20	0.0	3[e]	5.5	0.8±0.1	0.40	50km→ 4000km
	Rain Raingauge, time series[f]	0.5-0.7	.45-.60	0.0-0.1	2.5-3[g]	2.7-4	.75±.1	0.65±.15	8 minutes→16 days[h]
	Daily streamflow[i]	1.45±.3	0.2±.1	-0.1±.1	2.5±.5	2.5-4	0.6	0.3±.1	1month→30 years
ent ocity	Wind (tunnel, time)[j]	1.30	0.06	.33	—	8.7	—	—	1ms→ 1s
	Wind atmos. (time)[k]	1.45	0.07	.33	7.5±1	6.3	-0.1±.03	0.20±.03	1ms→ 1s
	Wind atmos. (horizontal)[l]	1.35±.07	0.068±.01	0.33±.03	7.0±1	7±0.5	-0.1±.02	0.22±.03	12m→12km
	Wind atmos. (vertical)[m]	1.85±.05	.076±.01	0.6±.1[n]	5±0.2[o]	4±0.2	0.07±.03	0.33±.03	50m→14km
ra- es	Climatological Temperatures	1.4[o2]	0.06[o2]	0.25[o3]	5[o3]	6.5	0.0	0.2	4→4,000years
	Temperature (atmos, time)[p]	1.20	0.04	0.30	5[q]	15	-0.2	0.1	0.1s→ 1000s
	Temperature, atmos. (hor.)[s]	1.25±.06	0.04±.01	33±.03[s2]	5.5[s3]	13	-0.2	0.10±.02	12m→12km
ent lars	Pollution (Seveso)[t]	1.2	0.8	-0.2	3[t2], 5[t3]	2.1	1.5-2	1.5-1.9	30m→5km
	Cloud liquid water (hor.)[u]	2.00±.01	0.07±.01[v]	0.28±.03[v]	2.2±0.1[v1]	3.8±0.1	-0.08±.05	0.15±.01	5m→330km
ring tworks	Density of stations[w]	0.8	0.3	0.0	3.6	11	0.6	0.6	200km→20000 km
es	Sea Ice (radar)[x]	1.85±.05	0.01±.01	-.15±.05	>5	17	—	—	50m→25km
	Ocean surface (0.95μm)[y]	1.1	0.25	0.35	3[z]	6.6	0.2	0.6	1m→50m
	Topography[aa]	1.8±.1	0.06±.01	0.5±.02	>5	7±0.5	—	—	50m→1000km
	Rock fracture surfaces[ab]	1.5	0.09	0.85	—	8	—	—	50μm→5cm
physics	Galactic luminoscity[bb]	1.2±0.4	1.3±0.1	0.0	1.35[bc]	1.5±0.1	1.8±0.1	1.5±0.1	0.1→100[o]
Earth	Seismicity[cc]	1.1	1.35	0.0	0.9[dd]	1.4	1.2	1.1±.1	2km→1000km
	Geomagnetic field[ee]	1.9	0.3	0.75	1.4	2.7	-0.14	0.4	400m→100km
ology	Low frequency speech[ff]	2.0	0.1	-0.35	—	3.2	—	—	0.1s→1000s

Table 1: Empirical estimates of universal multifractal parameters.

Key to Table 1

[a] Tessier et al. 1993a; see also Lovejoy et al. 1993
[b] The value of H depends slightly on the wavelength band used.
[b1] At 19, 21, 37GHz., Lavallée et al. 1993, the valuew of H depends slightly on the wavelength band used.
[c] Tessier et al. 1993a.
[c2] Calculated for a single realisation; $D_s = 0$.
[d] Schertzer and Lovejoy 1987, Duncan et al. 1993, Lovejoy 1981 obtained $q_D \approx 1.66$ for integrals of reflectivity of isolated storms
[e] Tessier et al. 1993a, using a global raingauge network, correcting for the multifractal sparseness of the network
[f] Tessier et al. 1993a, Ladoy et al. 1993 obtain similar values for the global network and Nimes respectively (for 12, 24 hour resolution respectively). Other similar values were obtained in Réunion and Dédougou, Hubert et al. 1993. Nguyen et al. 1993 find the slightly higher α, smaller C_1 in various locations near Montréal.
[g] Segal 1979 found a value of 2.5 ± 0.5 for 50 stations, 10 years of data at 5 minute resolution.
[h] Using a very large data base, Olsson 1994 finds similar values in Lund, Sweden, over periods of 8 minutes to 1 week.
[i] Tessier et al. 1993c, 50 rivers.
[j] Schmitt et al. 1992a, note that the theoretical (Kolmogorov) value of H is 1/3.
[k] Schmitt et al. 1993, 1994.
[l] Chiriginskaya et al. 1994.
[m] Lazarev et al. 1994, radiosondes.
[n] H was first estimated using Jimspheres, by Endlich and Mancuso 1968, and confirmed by Adelfang 1971, and Schertzer and Lovejoy 1985. The theoretical (Bogliano-Obhukov) value of H is 3/5.
[o] The value of q_D was first estimated in Schertzer and Lovejoy 1985.
[o2] F. Schmitt, S. Lovejoy, and D. Schertzer, analysis of Greenland ice core oxygen isotope ratios (in preparation).
[o3] Lovejoy and Schertzer 1986, analysis of hemispheric temperatures and ice core paleotemperatures.
[p] Schmitt et al. 1992b, the theoretical value for H is 1/3 if it is approximated as a passive scalar.
[q] This value was estimated for daily temperatures at individual stations (Lovejoy and Schertzer 1986a), regional averages (Ladoy et al. 1986).
[s] Chiriginskaya et al. 1994.

[s2] The theoretical value (passive scalar approximation) is 1/3.
[s3] In the vertical, Schertzer and Lovejoy 1985 estimate H=0.9, q_D=3.3 apparently for the potential temperture in the range 50m-6km.
[t] Salvadori et al. 1994.
[t2] This value was estimated for UF_6 tracer fluctuations by Visvanathan et al. 1991.
[t3] This value was estimated for CO_2 fluctuations over wheat fields Austin et al. 1991.
[u] Brosamlen et al. 1994.
[v] Davis et al. 1994 obtained similar values for H, C_1 with a smaller data set. The theoretical value (passive scalar approximation) is 1/3.
[v1] Due to the symmetry of the α=2 multifractal, the same value of q_D is obtained for 1/liquid water density.
[w] Using the global meteorological measuring network,considering the station density as a multifractal, Tessier et al. 1993,1994
[x] Synthetic aperture radar, 10, 30cm wavelengths, all polarizations, Francis et al. 1994.
[y] Tessier et al. 1993b.
[z] Kerman 1993.
[aa] Deadman's Butte Wyoming, 50m-25km; France 1km-1000km; Lavallée et al. 1993a.
[ab] F. Schmitt, private communication.
[bb] Garrido et al. 1994.
[bc] Schertzer et al. 1993.
[cc] Hooge et al. 1993, 1994.
[dd] This is the well-known Gutenberg-Richter exponent, first estimated by Gutenberg-Richter 1944, and is somewhat variable, the value cited here is for the Parkfield region.
[ee] Lovejoy et al. 1994.
[ff] Larnder et al. 1992.

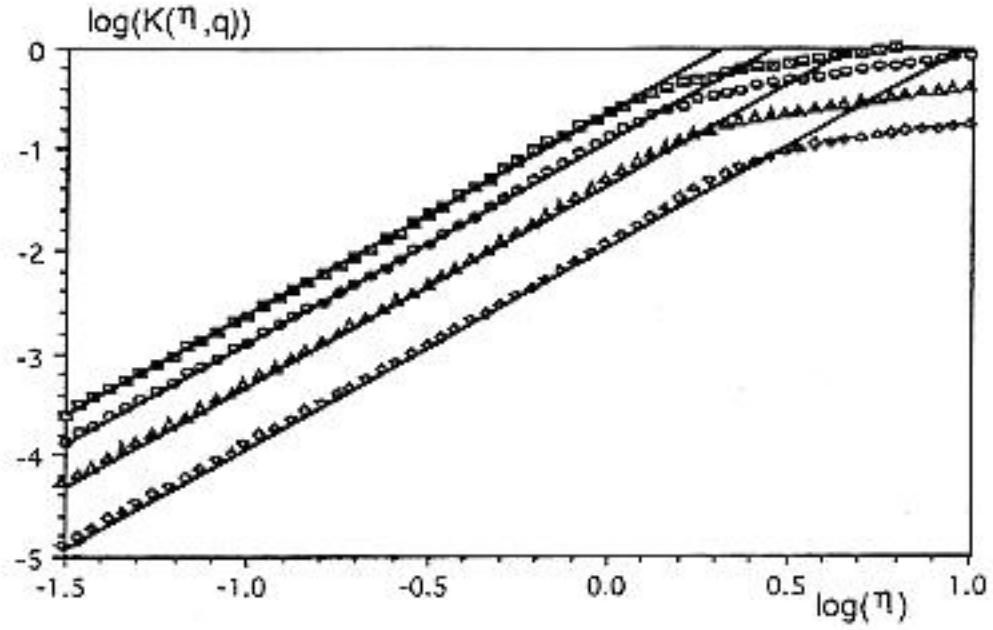

Figure 12: $K(q,\eta)$ as a function of η on $\log_{10} - \log_{10}$ scales, for the values (top to bottom) q =2.5, 2.0, 1.5, 0.75. As expected for universal multifractals, the curves are linear and parallel for a certain range of the moments α. The parameter α can be identified as the slope of the straight line parts of the curves, whereas C_1 is the value of the straight line at the intersection $\eta = 0$. From Brosamlen et al. 1994.

3.2 Isotropic (self-similar) simulations of universal multifractals

We now indicate briefly how to exploit the universality (and the measured H, C_1, α parameters) to perform multifractal simulations. The first multifractal models of this type were discussed in Schertzer and Lovejoy 1987, and Wilson et al. 1991 give a comprehensive discussion including many practical (numerical) details. In particular, the latter describes the numerical simulation of clouds and topography, including how to iteratively 'zoom' in, calculating details to arbitrary resolution in selected regions. Pecknold et al. 1993 give a number of improvements and include more systematic results (including those shown here). Although we will not repeat these details, enough information has been given in the previous sections to un-

derstand how they work.

First, for a conserved (stationary) multifractal process ϕ_λ we define the generator $\Gamma_\lambda = \log \phi_\lambda$. To yield a multifractal ϕ_λ, it must be exactly a $1/f$ noise, i.e., its spectrum is $E(k) \approx k^{-1}$ (this is necessary to ensure the multiple scaling of the moments of ϕ_λ). To produce such a generator, we start with a stationary gaussian or Levy 'subgenerator'. The subgenerator is a noise consisting of independent random variables with either gaussian (α=2) or extremal Levy distributions (characterized by the Levy index α), whose amplitude (e.g., variance in the Gaussian case) is determined by C_1. The subgenerator is then fractionally integrated (power law filtered in Fourier space) to give a k^{-1} spectrum. This generator is then exponentiated to give the conserved ϕ_λ which will thus depend on both C_1 and α. Finally, to obtain a non conserved process with spectral slope β, the result is fractionally integrated by multiplying the Fourier transform by k^{-H} where H is given in eq. 9. The entire process involves two fractional integrations and hence four FFT's. 512 x 512 fields can easily be modelled on personal computers (they take about 3 minutes on a Mac II), and 256 x 256 x 256 fields (e.g., space-time simulations of dynamically evolving multifractal clouds) have been produced on a Cray-2 (Brenier 1990, Brenier et al. 1990).

Figures 13-18 inclusive show series of one dimensional simulations with various parameters.

It is apparent from them that C_1 is the measure of the sparseness of the field: the higher the C_1, the fewer the field values corresponding to any given singularity. (Because the field is normalized, the spikes are higher for the fields with higher C_1). It is also again apparent that the higher α fields are dominated by a few large singularities.

4 Elements of Generalized Scale Invariance (GSI)

4.1 Discussion

The usual approach to scaling is first to posit (statistical) isotropy and only then scaling, the two together yielding self-similarity. Indeed this approach is so prevalent that the terms scaling and self-similarity are often used interchangeably! Perhaps the best known example is Kolmogorov's hypothesis of 'local isotropy' from which he derived the $k^{-\frac{5}{3}}$ spectrum for the wind fluctuations. The GSI approach is rather the converse: it first posits scale invariance (scaling), and then studies the remaining non-trivial

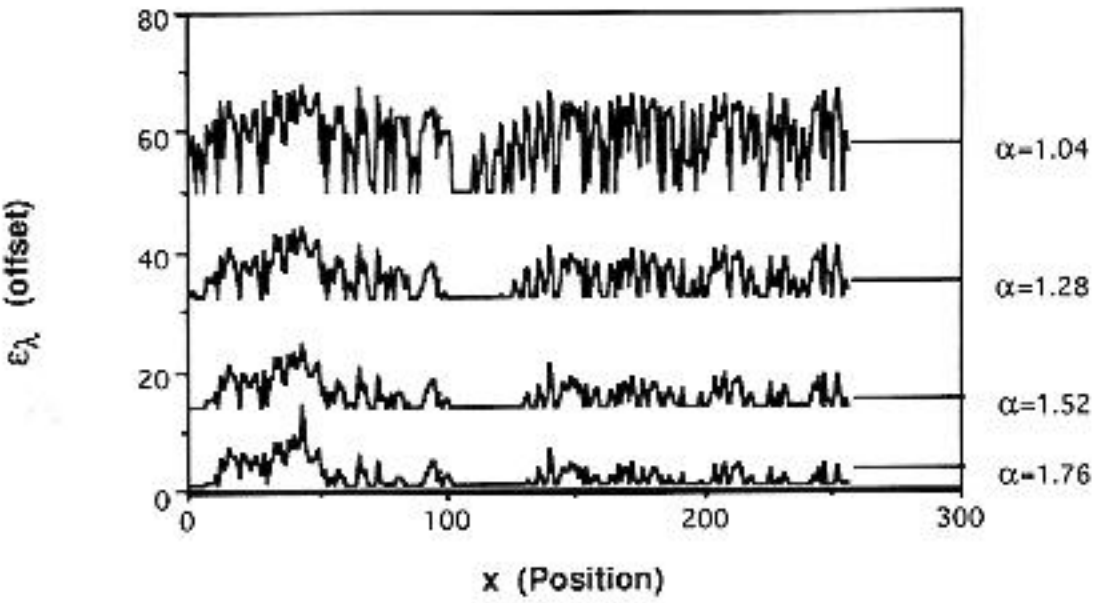

Figure 13: One-dimensional simulation of length 256, with $C_1 = 0.9$ and varying α These simulations have been vertically offset so as not to overlap. From Pecknold et al. 1993.

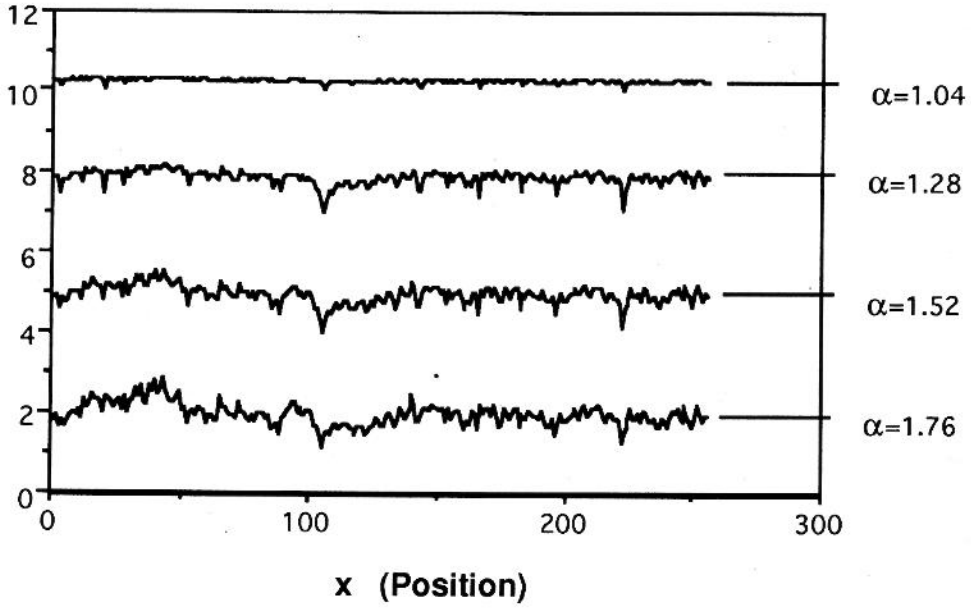

Figure 14: One-dimensional simulation of length 256, with $C_1 = 0.01$ and varying α These simulations have been vertically offset so as not to overlap. From Pecknold et al. 1993.

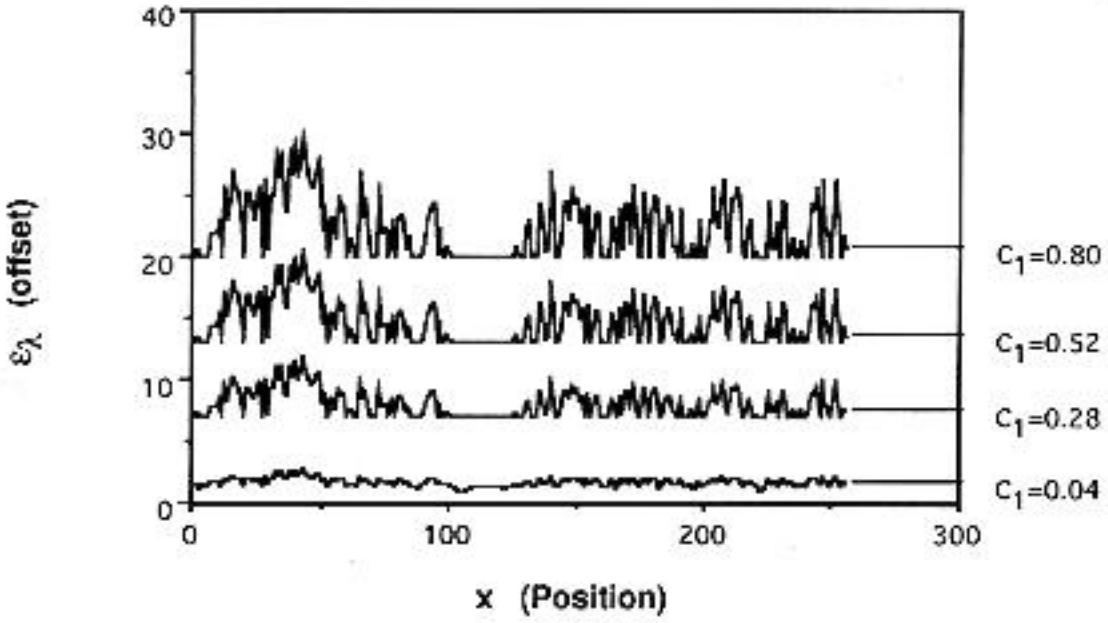

Figure 15: One-dimensional simulation of length 256, with $\alpha = 1.4$ and varying C_1 These simulations have been vertically offset so as not to overlap. From Pecknold et al. 1993.

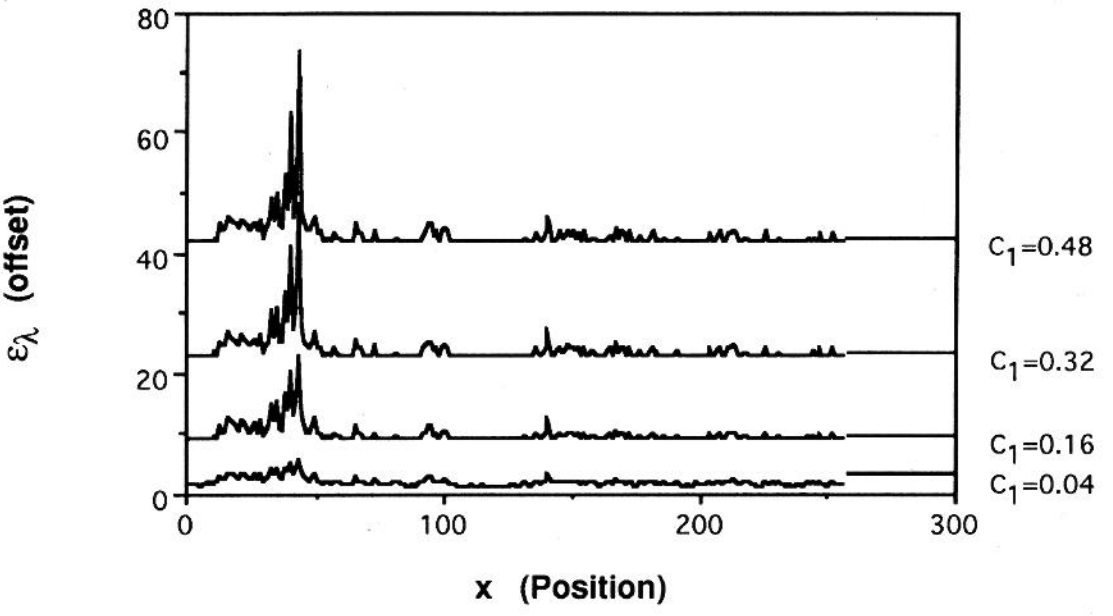

Figure 16: One-dimensional simulation of length 256, with $\alpha = 2.0$ and varying C_1 These simulations have been vertically offset so as not to overlap. From Pecknold et al. 1993.

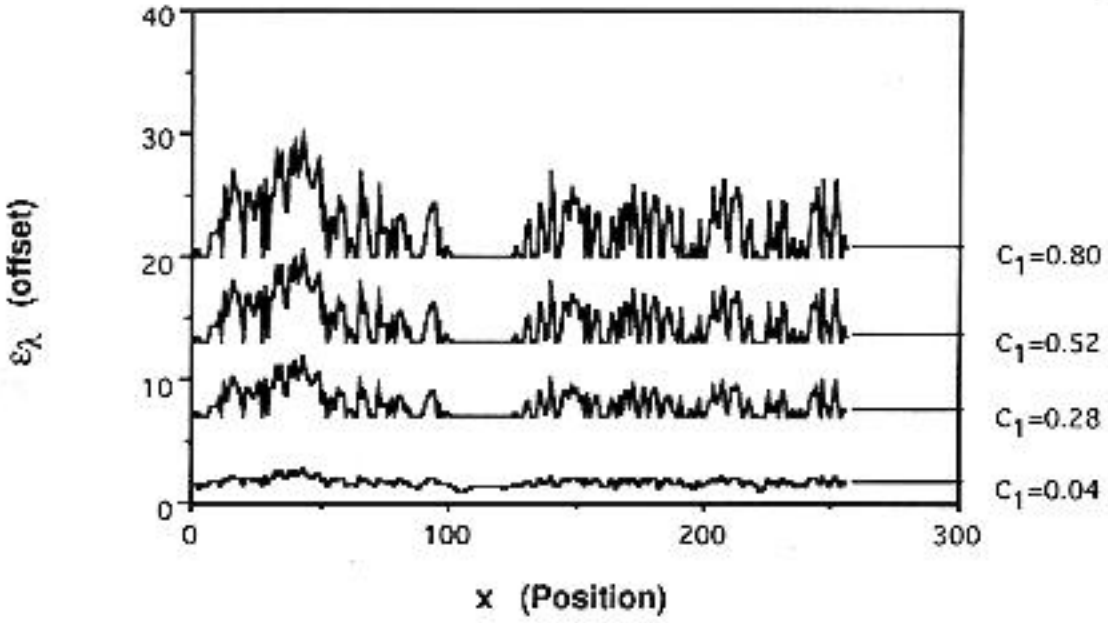

Figure 15: One-dimensional simulation of length 256, with $\alpha = 1.4$ and varying C_1 These simulations have been vertically offset so as not to overlap. From Pecknold et al. 1993.

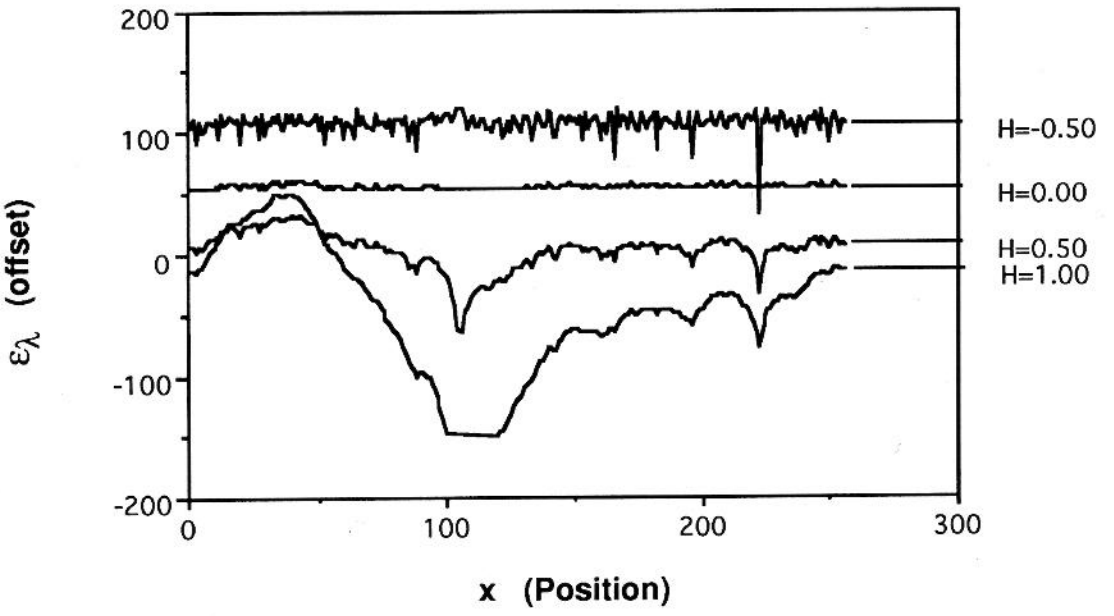

Figure 18: One-dimensional simulation of length 256, with $\alpha = 1.5$ and $C_1 = 0.4$, fractionally integrated with varying H (non-conservation parameter). These simulations have been vertically offset so as not to overlap. From Pecknold et al. 1993.

symmetries. For instance, fig. 1 gives a (scaling) anisotropic version of the usual isotropic cascade scheme (in which the rectangles in fig. 1 would be replaced by squares). One may easily check that this type of anisotropy - which reproduces itself from scale to scale - does not introduce any characteristic scale. The straightforward generalization of scaling shown in fig. 1 involving scaling anisotropy in a fixed direction is called 'self-affinity'. As far as we know this anisotropic scheme (Schertzer and Lovejoy 1983) seems to be the first explicit model of a physical system involving a fundamental self-affine fractal mechanism.

4.2 The basic elements of GSI

Consider scale invariance under, isotropic dilations/contractions (e.g., simple reductions): $\lambda^{-1}B = T_\lambda B$ where T_λ is a scale changing operator. In our example, $T_\lambda = \lambda^{-1}\mathbf{1}$ where $\mathbf{1}$ is the identity matrix. This means that if $\mathbf{x}_1$ is an element in B then $\mathbf{x}_\lambda = T_\lambda \mathbf{x}_1$ (again, in the previous example $T_\lambda = \lambda^{-1}\mathbf{1} \Rightarrow \mathbf{x}_\lambda = \lambda^{-1}\mathbf{x}_1$). The subscripts on $\mathbf{x}$ indicate the scale. In generalized scale invariance (GSI), T_λ can be much more general than isotropic dilations. Fig. 19 shows a generalized 'blow' down of the acronym 'NVAG' showing how the reduction is combined with stretching and rotation. In general, a scale invariant system will be one in which the small and large scales are related by a scale changing operation that involves only the scale ratios; there is no characteristic size. In what follows we outline the basic elements necessary for defining such a system: we follow closely the development in Schertzer and Lovejoy 1985b.

To be completely defined, GSI needs more than a scale changing operator; it also requires a definition of the unit scale, as well as a deinition of how to measure the scale. These three basic elements can be summarized as follows:

(i) The unit ball B_1 which denes all the unit vectors. If an isotropic ball (e.g., circle or sphere) exists, we call the corresponding scale the 'spheroscale'. For simplicity we often assume this - indeed direct evidence for this exists in many satellite cloud pictures, but it is not strictly necessary (and at least in some cases not at all true!).

(ii) The scale changing operator T_λ which transforms the scale of vectors by scale ratio λ. T_λ is the rule relating the statistical properties at one scale to another and involves only the scale ratio (there is no characteristic 'size'). This implies that T_λ has certain properties. In particular, if and

Figure 19: A generalized blow-down with increasing λ of the acronym 'NVAG'. If $\mathbf{G} = \mathbf{I}$, we would have obtained a standard reduction, with all the copies uniformly reduced converging to the centre of the reduction (thanks to S. Pecknold, G. Lewis). Here the parameters determining $\mathbf{G}$ are $c = 0.3$, $f = -0.5$, $e = 0.8$ (see section 4), and each successive reduction is by 28

only if $\lambda_1 \lambda_2 = \lambda$, then

$$B_\lambda = T_{\lambda_1} B_{\lambda_2} = T_{\lambda_2} B_{\lambda_1} \tag{13}$$

i.e., T_λ has the group properties (see fig. 20):

$$T_{\lambda_2} T_{\lambda_1} B_1 = B_\lambda = T_{\lambda_1} T_{\lambda_2} B_1 \tag{14}$$

Hence T_λ is a one parameter multiplicative group $\Rightarrow T_\lambda = \lambda^{-G}$, where G

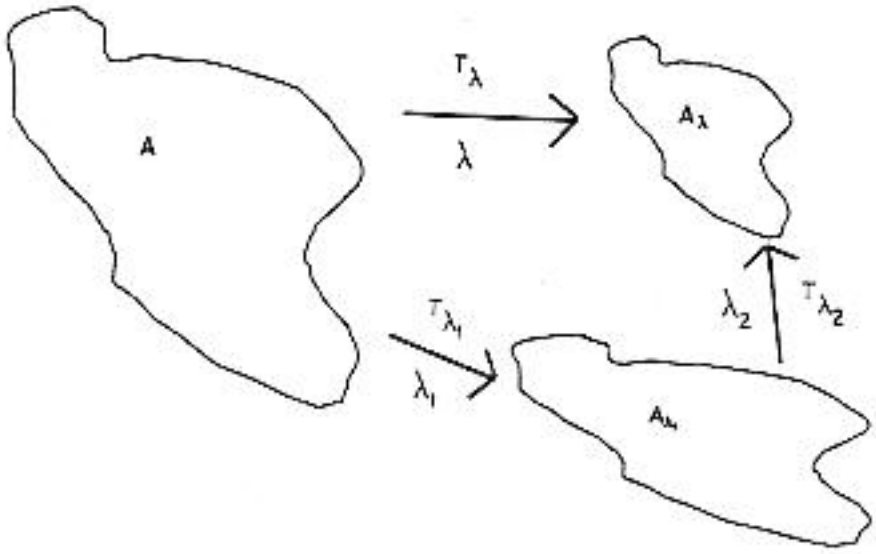

Figure 20: Illustration of the group property of the scale changing operator. From Schertzer and Lovejoy 1994.

is the generator of the group. We use the negative sign since in future we will be only interested in reductions by factor λ since we shall see that in turbulent cascades, energy flux is transferred from large to small scales (T_λ will *reduce* sizes by factor λ). We will not require that inverse operators $T_\lambda^{-1} = T_{\lambda^{-1}}$ exist, hence we really only have a semi-group (the inverse will however usually exist if G is a matrix).

4.3 Linear GSI and differential rotation: the example of the Coriolis force

In the atmosphere, one expects differential rotation (associated with the Coriolis force $\Omega \wedge \mathbf{v}$, associated for example with cloud texture) as indicated

above. This can be modelled by a matrix G with off-diagonal elements. To understand this, we decompose G into quaternions (or equivalently, Pauli matrices):

$$G = d\mathbf{1} + e\mathbf{I} + f\mathbf{J} + c\mathbf{K} \tag{15}$$

where

$$\mathbf{1} = \begin{bmatrix} 1 & 0 \\ 0 & 1 \end{bmatrix}, \quad \mathbf{I} = \begin{bmatrix} 0 & -1 \\ 1 & 0 \end{bmatrix} \tag{16}$$

$$\mathbf{J} = \begin{bmatrix} 0 & 1 \\ 1 & 0 \end{bmatrix}, \quad \mathbf{K} = \begin{bmatrix} -1 & 0 \\ 0 & 1 \end{bmatrix} \tag{17}$$

These matrices satisfy the following anticommutation relations:

$$\{\mathbf{I}, \mathbf{J}\} = 0, \quad \{\mathbf{I}, \mathbf{K}\} = 0, \quad \{\mathbf{J}, \mathbf{K}\} = 0 \tag{18}$$

Writing $u = \ln \lambda$ and $a^2 = c^2 + f^2 - e^2$ we obtain:

$$T_\lambda = \lambda^{-G} = \lambda^{-d}\lambda^{(G-d1)} = \lambda^{-d}\left[\mathbf{1}\cosh(au) - (G - d\mathbf{1})\frac{\sinh(au)}{a}\right] \tag{19}$$

When $a^2 < 0$, the above formula holds but with $|a|$ replacing a and ordinary trigonometric functions rather than hyperbolic functions. The case $a^2 > 0$ corresponds to domination by stratication, whereas $a^2 < 0$ to domination by rotation. Examples of both balls and trajectories (the locus of points $\mathbf{r}_\lambda = \mathbf{T}_\lambda \mathbf{r}_1$, obtained by λ varying with $\mathbf{r}_1$ fixed) are shown in fig.21. To take into account the spatial variation of anisotropy, the generator can be taken to be a nonlinear function, or even stochastic (fig. 22).

5 Multifractal simulations for solving problems in remote sensing, some examples

5.1 Resolution independent algorithms

We are rarely able to directly remotely sense the fields of interest. Typically, a satellite will observe radiances associated with a field and then (often complex) semi-empirical algorithms are used to try to infer the various physical characteristics from the radiances. Above we argued that such algorithms must at a minimum explicitly take the resolution into account, preferably removing it entirely so as to obtain sensor independent algorithms. Ultimately however, a full understanding of the relationship

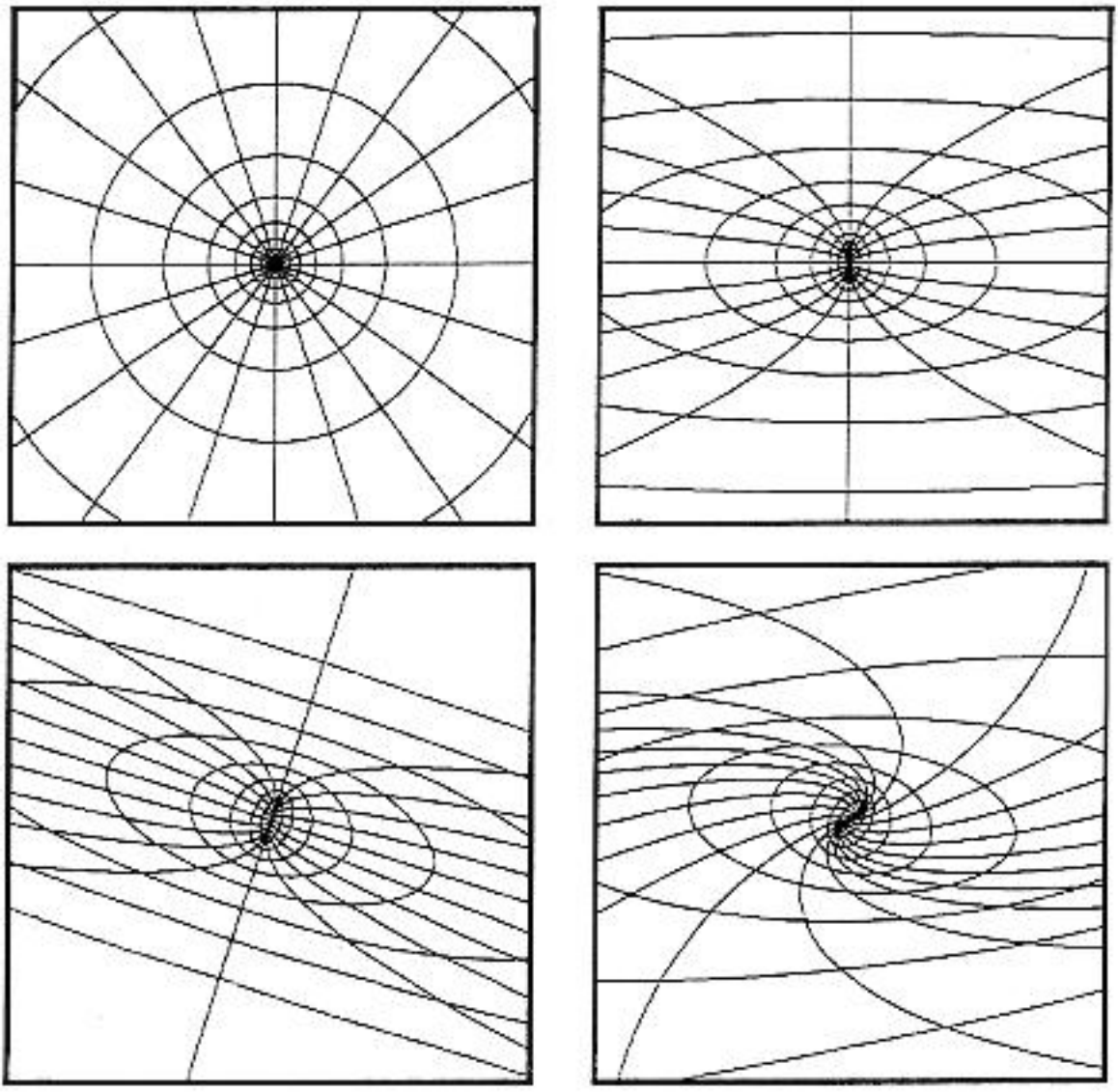

Figure 21: Examples of balls and trajectories for linear GSI with sphero-scale. Isotropic case: $c = 0.0$, $f = 0.0$, $\epsilon = 0.0$ (top left); self-affine case: $c = 0.35$, $f = 0.0$, $\epsilon = 0.0$ (top right); stratification dominant case ($a^2 > 0$) with no rotation: $c = 0.35$, $f = 0.25$, $\epsilon = 0.0$ (bottom right); rotation dominant case ($a^2 < 0$): $c = 0.35$, $f = 0.25$, $\epsilon = 0.6$. For all cases $d = 1$ with sphero-scale at 30 units (pixels) out of a total of 512. From Lewis 1993.

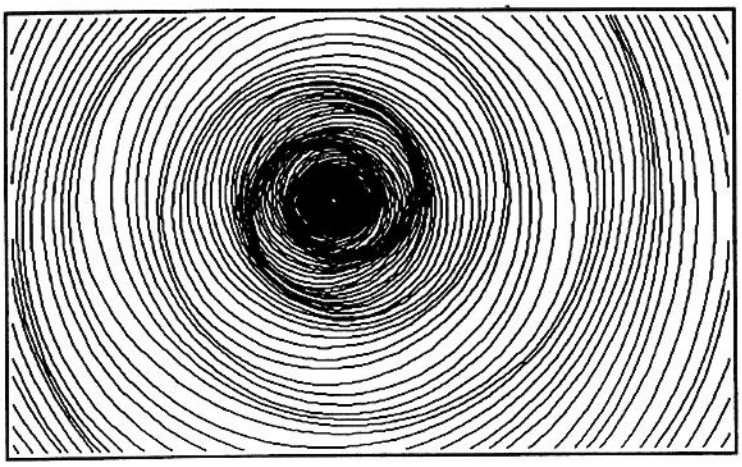

Figure 22: Deterministic non-linear GSI with a stochastic generator. Schertzer and Lovejoy, 1991.

between the remotely sensed and underlying physical field will only be possible as the result of explicit multifractal modelling of the radiation/matter interaction. Our efforts in this direction have been especially aimed at studying these issues in the rain and cloud fields since radar data of rain and satellite data of clouds are probably the data sets with the widest range of spatial and temporal scales available anywhere.

5.2 Scattering statistics in multifractal clouds

We have argued that over wide ranges, atmospheric fields may be expected to display strong multifractal variability. In a series of papers (Gabriel et al. 1986, Lovejoy et al. 1988, Lovejoy et al. 1990, Gabriel et al. 1990, Davis et al. 1990), we argued that scaling models involving 'monofractal' clouds do in fact already display interesting and realistic radiative properties. In particular, formulae for asymptotically optically thick clouds were derived and were shown to provide straightforward explanations for the 'albedo paradox'. Davis et al. 1991a,b obtained some early results on more realistic multifractal clouds, including theoretical formulae for small distance behaviour, as well as supercomputer simulations. Cahalan 1989, 1994 and Barker and Daies 1992 studied optically thin monofractal clouds and Evans

1993 performed numerical simulations on optically thin multifractal clouds.

Here we give a glimpse at some more recent results which may provide the basis for systematic study of radiative transport in multifractal media. Specifically, we indicate how formulae analogous to eqs. 2, 3 for the multifractal optical density field arise for radiative properties. Consider the following definitions:

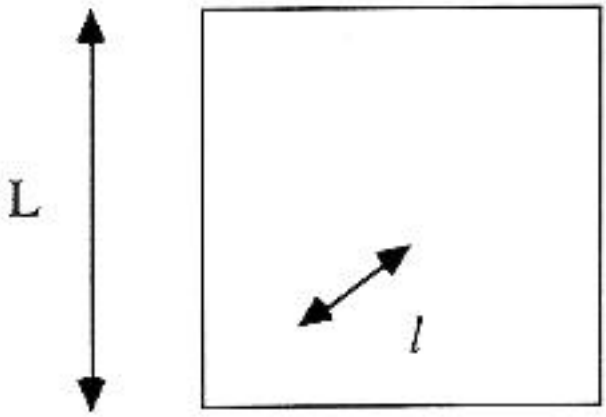

k= extinction coefficient $[m^2 kg^{-1}]$
$\langle\rho\rangle$ = mean cloud density $[kgm^{-3}]$
l = random photon path distance $[m]$
L= size of cloud $[m]$
l_m= mean free path (m.f.p.) of a photon in the equivalent homogeneous cloud = $(k\langle\rho\rangle)^{-1}$ $[m]$
$x = \frac{l}{L} = l^{-1}$ random photon distance, (fraction of cloud)
$\tau_p = \frac{l}{l_m}$ = random photon distance, (no. of m.f.p.'s = kx)
$\lambda = \frac{L}{l}$ = scale ratio $\leq \Lambda$, (Λ = maximum cascade resolution)
$\kappa = \frac{L}{l_m}$ = extinction parameter = no. of m.f.p.'s across cloud = mean optical depth = extinction coefficient in units such that $L = 1, \langle\rho\rangle = 1$.

Detailed analysis (Lovejoy et al. 1994b) of radiative transfer in multifractal clouds indicates that in a cloud whose large scale mean optical depth is κ that the photon optical path statistics can be described by a formalism extremely similar to the multifractal density statistics but with κ playing

the role of resolution λ. First, the optical distance between

$$\tau(l) = \int_l k\rho_\Lambda(z')dz' = k\rho_{l,d}l \tag{20}$$

where we have written ρ_l for the average density at resolution l. Using the above notation, we obtain:

$$\tau = \frac{\rho_\lambda}{\langle\rho\rangle}\lambda^{-1}\frac{L}{l_m} = \lambda^{\gamma-1}\kappa \tag{21}$$

which is the optical thickness over a distance l through a singularity of order γ. The direct (unscattered) transmission T across this distance is thus:

$$T(l) = e^{-\tau(l)} \tag{22}$$

Since the transmittance is the probability distribution for photon path lengths, we can average over the singularities, and obtain:

$$Pr(l' > l) = \langle T(l)\rangle = \langle e^{-\tau(l)}\rangle \tag{23}$$

Take τ_p as the dimensionless photon path and write it as a function scaling with an 'order of singularity γ_p' defiined as follows:

$$\tau_p = \kappa^{\gamma_p} = \frac{l}{l_m} = \kappa x = \kappa\lambda^{-1} \tag{24}$$

or:

$$\lambda = \kappa^{(1-\gamma_p)} \tag{25}$$

We can now obtain a multifractal scattering formalism in which the extinction coefficient κ takes the place of the scaling parameter λ. Instead of the codimension function $c(\gamma)$ of the singularities of the cloud density γ we rather talk about an analogue codimension function $c_p(\gamma_p)$ which describes how the single photon path distance singularity γ_p varies with the extinction coefficient:

$$Pr(\tau_p \geq \kappa^{\gamma_p}) = Pr(l' > l) \approx \kappa^{-c_p(\gamma_p)} \tag{26}$$

$$\left\langle \tau_p^{q_p} \right\rangle \approx \kappa^{K_p(q_p)} \tag{27}$$

and anticipate that the two will be linked by a Legendre transform as in the standard multifractal case. The mean transmission in equation 23 is

obtained by averaging over the singularities, using eq. 2 to obtain the probability density of γ:

$$\kappa^{-c_p(\gamma_p)} \approx \langle T(\gamma,\lambda)\rangle = \int_{-\infty}^{\infty} e^{-\tau(\gamma,\lambda)} p(\gamma,\lambda) d\gamma \tag{28}$$

$$= \int_{-\infty}^{1} e^{-\kappa\lambda^{\gamma-1}} \lambda^{-c(\gamma)} d\gamma = \int_{-\infty}^{1} \kappa^{-\frac{\alpha\gamma}{\log\kappa} - c\left(1-\frac{1-\gamma_z}{1-\gamma_p}\right)(1-\gamma_p)} d\gamma_z \tag{29}$$

where we have introduced the tranformation of variables:

$$1-\gamma = \frac{1-\gamma_z}{1-\gamma_p} \tag{30}$$

In the lognormal case, the above integral can be done exactly; more generally, we can use the method of 'moving maximum' to obtain an asymptotic estimate of the integral by considering where the maximum occurs. This method will work as long as the latter is well-defined. This in turn hinges upon the existence of a solution to the following equation obtained by equating the γ_z derivative to zero:

$$\kappa^{\gamma_z} = -c'(\gamma) = -q \tag{31}$$

where the q is the Legendre conjugate of γ, it is the corresponding moment of the density distribution. We see immediately, that some $c' < 0$, must exist, i.e some negative moments must exist. While this seems rather general, in fact for universal multifractals, it is only true of the lognormal multifractal, all other universals have divergent moments for all negative moments. Assuming that the moments do exist, we obtain two families of codimension and moment scaling functions; their mutual relations are given in table 2.

Photon statistics	Cloud statistics
q	$= -q + K(q)$
$K_p(q_p) = max_{\gamma_p}[q_p\gamma_p - c_p(\gamma_p)]$	$= K(q) = max_\gamma[q\gamma - c(\gamma)]$
$1-\gamma_p$	$= \frac{1}{1-\gamma}$
$c_p(\gamma_p) = max_q[q\gamma_p - K_p(q_p)]$	$= \frac{c(\gamma)}{1-\gamma} = \frac{max_q[q\gamma - K(q)]}{1-\gamma}$

Table 2: Summary of relations between multifractal cloud and photon scattering exponents

To give an example of the above, consider the $\alpha = 2$ (lognormal multifractal). We have:

$$c(\gamma) = C_1 \left(\frac{\gamma}{C_1} + 1 \right)^2 \tag{32}$$

$$c_p(\gamma_p) = \frac{(1 - (1 + C_1)(1 - \gamma_p))^2}{4C_1(1 - \gamma_p)} \tag{33}$$

$$K(q) = C_1(q^2 - q) \tag{34}$$

$$K_p(q_p) = q_p - \frac{\sqrt{(1 + C_1)^2 + 4C_1 q_p} - (1 + C_1)}{2C_1} \tag{35}$$

Numerics have shown (Brosamlen 1994) that these formulae are accurate even for clouds with mean optical thickness of the order of 4-10. Since the $K_p(q_p)$ function is linear in homogeneous clouds, and the above $K_p(q_p)$ function is close to linear -especially near $q_p = 0$ which corresponds (see table 2) to the most probable photon path and singularity, we can use the above to approximately 'renormalize' the cloud, obtaining an effective extinction parameter:

$$\kappa_{\text{eff}} \approx \kappa^{\frac{1}{1+C_1}} \tag{36}$$

This result quite accurately predicts the numerical estimates of transmission through multifractal clouds discussed in the next section, and the exponent is the same as that obtained for anomalous difusion in lognormal multifractals (also below). In a forthcoming paper (Lovejoy et al. 1994), we give many more details and extensions to multiple scattering.

Finally, a full understanding of the cloud radiation interaction involves a detailed understanding of the relation between cloud and radiation singularities. This is the subject of a paper by Naud et al. 1994.

5.3 Visible light scattering in multifractal clouds

To further understand the relations between the cloud and radiation fields, we seek to statistically relate the multifractal singularities of the various fields. From a numerical point of view, this is very demanding. Monte Carlo techniques avoid this problem, but require enormous numbers of simulated photons in order to yield good estimates of the internal cloud fields.

In optically thick clouds, photons undergo many scatterings and the details of the scattering phase function is not too important (according to the monofractal studies - Lovejoy et al. 1990, Gabriel et al. 1990, Davis et al. 1990 - it will affect prefactors, not exponents). In order to concentrate study on the effect of inhomogeneity, and to simplify calculations, a

two dimensional system was studied with phase functions which only permit scattering through 90 degrees; (discrete angle -DA- radiative transfer) the radiances decouple into non-interacting families with only four radiace directions each (details in Davis et al. 1991a). The phase functions were position independent; for simplicity we used isotropic DA phase functions. For validation purposes, the calculations were made using both Monte Carlo and relaxation techiques. The four radiances were then used to calculate the total radiance, the vertical and horizontal fluxes, as well as a component characterizing the anisotropy of the field. By varying the extinction coefficient, we were able to study the effect of increasing cloud thickness, optical thicknesses between 12 and 195. The calculations were performed on large (1024 x 1024 point grids using the Cray-2. at Palaiseau, France. The main conclusions were:

(1) Horizontal fluxes were typically less than 10radiance fields were close to plane parallel, even though globablly the radiative response was far from plane parallel.

(2) The anisotropic component was often very large; this points to the importance of 'streaming' or 'channelling' of photons through the more tenuous regions. It also indicates that the diffusion approximation will be poor even in optically thick clouds.

(3) The overall trasmittences were compared with those of equivalent plane parallel clouds and with those obtained using the independent pixel approximation (each column independent).

The agreement was generally poor, although the independent pixel approximation was much better than the plane-parallel approximation. Such effects could readily account for the 'albedo paradox' (divergences of factors of ten or more between plane parallel and in situ estimates of cloud liquid water).

5.4 Diffusion on multifractals

The simplest nontrivial transport process in multifractals is diffusion and the diffusion equation is often taken as a simplified radiative transport model. Using this approximation, and taking J as the total intensity and $D(\underline{x})$ as the (multifractal) diffusion constant, we have:

$$\nabla.(D(\underline{x})\nabla J) = \frac{\partial J}{\partial t} \tag{37}$$

where again, the diffusion constant is related to the cloud properties via:

$$D(\underline{x}) = \frac{1}{k\rho(\underline{x})} \tag{38}$$

where (as above) k is the extinction coefficient, and $\rho(\underline{x})$ is the multifractal cloud density. In one dimension, many aspects are particulary simple. For example, the steady state J is a multifractal since:

$$\frac{\partial}{\partial x}\frac{1}{k\rho(x)}\frac{\partial J}{\partial x} = 0 \tag{39}$$

which implies:

$$\frac{\partial J}{\partial x} = k\rho(x) \tag{40}$$

i.e. $J(x)$ will be multifractal with conservation parameter H (see eq. 9) increased by one (since J is an integral order one of the density, and H specifies the degree of fractional integration necessary to obtain the field froom a conserved multifractal). The time dependent case is less straightforward, but still can be solved -at least in 1-D - (for details, see Silas et al. 1994). Because of the scaling, we anticipate that for photon random walks, the distance r after time t will vary as:

$$\langle r^q(t)\rangle = t^{S(q)} \tag{41}$$

where $S(q)$ is the walk scaling exponent. Since the walk is an additive (monofractal) process, $S(q)$ will be linear, defining as usual the 'walk dimension' d_w we have:

$$S(q) = \frac{q}{d_w} \tag{42}$$

In one dimension, Silas et al. 1994 obtain the following result which (when applicable, i.e. K(-1) is finite), is believed to be exact:

$$d_w = 2 + K(-1) \tag{43}$$

In the above, the dressed scaling exponent K is used; since this is always positive, $d_w > 2$, hence the photon walk is subdiffusive ('normal' diffusion has $d_w = 2$; here, the photon gets partially 'trapped' between large singularities, this subdiffusive behaviour was noted in a numerical example studied by Meakin 1987). Eq. 43 shows that as expected from the monofractal behaviour of the path, only a single multifractal singularity is important for the walk ($\gamma_{cr} = K'(-1)$). Indeed, the critical role of this singularity can be considered to produce a dynamical 'phase' transition, since truncating the high multifractal singularities (γ) has no effect on the transport. As long as $\gamma > \gamma_{cr}$, the transport is anomalous, becoming 'normal' discontinuously for $\gamma < \gamma_{cr}$.

5.5 Radar reflectivity of multifractals 'speckle'

Radar remote sensing of sea ice, ocean or land surface or rain involves inhomogeneities due to multifractal structures that extend down below not only radar pulse volumes but also below microwave wavelengths (Lovejoy and Schertzer 1990a,b, Duncan et al. 1993). This leads to the 'speckle' phenomenon whereby small changes in look angle will be associated with large changes in intensity. It also implies that the usual way of removing this effect (by assuming subpulse volume statistical homogeneity and hence incoherent scattering) will lead to systematic errors. To correct the standard theory for these effects, we can model the reflector as a multifractal distribution of dielectrics. In the simplest case appropriate for rain, a scalar approximation is sufficient for most purposes since the scattering from drops is nearly isotropic. Other situations such as sea ice will involve mutifractal distributions of dielectric tensor and will require the formalism of Lie cascades (Schertzer and Lovejoy 1993).

Actually, even for the scalar case basic results can be obtained using complex (Lie) cascades, since the radar detects a (complex) Fourier component. To see this consider a one (spatial) dimensional distribution of radar scatterers $\sigma_\Lambda(x,t)$, varying in time, with an inner (dissipation scale) Λ^{-1}, the radar number is $k/2$ (the factor 2 is for simplicity; it will take into account the round trip distance to the scatterers), and the pulse volume is length λ^{-1}. We will be taking the outer scale of the process to be 1, hence we will be interested in $\lambda > 1$. Similarly, we will use units such that the velocity is unity (it is assumed to be independent of scale, we use isotropic space/time). The spatial average of the amplitude of the reflected wave is:

$$A_\lambda(k) = \frac{1}{\lambda^{-1}} \int_0^{\lambda^{-1}} e^{ikx} \sigma_\Lambda(x) dx \tag{44}$$

If we consider $e^{ikx}\sigma_\Lambda(x)$ $(k < \Lambda)$ as a complex (bare) cascade quantity, then, for $\lambda \ll k < \Lambda$, $A_\lambda(k)$ is simply a dressed complex cascade. Using results on complex cascades, we obtain

$$Re(K_A(q)) = K_\sigma(q) + qC_{1,R} \tag{45}$$

where only $C_{1,R} = Re(K_A(1))$ remains to be determined. This result has been tested numerically by Duncan 1993, Duncan et al. 1994 and indicated that the statistics of the cross-section field $(\sigma, K_\sigma(q))$ and the modules of the amplitude $(|A|, Re(K_A(q))$ are the same except for a term linear in q which represents a scale dependent bias. By using space-time transformations, it is also possible to model the temporal behaviour of the reflectivity field. Duncan et al. 1994 shows excellent agreement is found with rain data.

6 Conclusions

We have summarized a growing body of work indicating that - as theoretically predicted - due to underlying nonlinear but scale invariant dynamics, that many geophysical fields are multifractal over substantial ranges of scale. This implies that they are strongly dependent on the resolution at which they are observed and that remote sensing algorithms must systematically remove these effects if sensor independent measurements of geophysical fields are to be obtained.

We also summarized the basic properties of multifractals. Although the properties of multifractals are more fully discussed in the accompanying paper SL94, we concentrate on the discovery of universal multifractals. In particular universality classes exist in which most of the details of the details of the dynamics are 'washed out' leaving a dependence on just three basic universal parameters. Without such universality classes, multifractals would be sensitive to an infinite numer of model paramters and would have little use. We summarised the empirical evidence for these two distinct properties in over 20 geophysical fields (many of them remotely sensed).

We also indicated that since scale invariance is a dynamical symmetry principle, it may be expected to hold widely; however, the scale changing operator will generally not be isotropic, hence we do not expect to observe self-similar multifractals and estimates of the generator of the scale changing operator using the Scale Invariant Generator technique confirm this. However, by allowing for very general (even stochastic) generators, we can take into account the observed texture and morphology of geophysical processes.

We also showed how to simulate multifractal fields, and we examined some of their properties. We argued that a full understanding of the relation between physically interesting quantities, and the remotely sensed radiances will require the use of such models, and we illustrated these ideas on radiative and diffusive transport, as well as on the problem of radar speckle.

7 Acknowledgments

We thank G. Brosamlen, Y. Chiriginskaya, A. Davis, N. Desaulniers-Soucy, M. Duncan, F. Francis, H. Gaonac'h, C. Hooge, P. Hubert, P. Ladoy, A. Lazarev, D. Lavallée, C. Naud, S. Pecknold, F. Schmitt, J. Todeschuk, and B. Watson for helpful comments, discussion and techical assistance.

8 References

[1] Adelfang, S. I. 1971, On the relation between wind shears over various intervals, J. Atmos. Sci., 10, 138.

[2] Austin, L. B., Austin, G. L., Schuepp, P. H., Saucier, A. 1991, Atmospheric boundary layer variability and its implication for CO2 flux measurements. In Non-linear Variability in Geophysics: Scaling and Fractals. Kluwer, D. Schertzer and S. Lovejoy ed.s, pp. 269-278.

[3] Bak, P., Tang, C. and Weiessenfeld, K. 1987, Self-Organized Criticality: An explanation of $1/f$ noise. Phys. Rev. Lett 59, 381-384.

[4] Barker H. W. and Davies, J. A. 1992, Solar Radiative Fluxes for Stochastic, Scale-invariant Broken Cloud Fields, J. Atmos. Sciences, 49, 1115-1126.

[5] Brax, P. and Pechanski, R. 1991, Levy stable law description on intermittent behaviour and quark-gluon phase transitions. Phys. Lett. B 253, 225-230.

[6] Brenier, P. 1990, Simulation dynamique multifractale des nuages, Master's thesis, Ecole Nationale supérieure de techniques avancées, Paris, France.

[7] Brenier, P., Schertzer, D., Sarma, G., Wilson, J. and Lovejoy, S. 1990, Continuous multiplicative cascade models of passive scalar clouds. Annales Geophysicae 8 (special edition), 320.

[8] Brosamlen, G., 1994, Radiative transfer in lognormal multifractal clouds and analysis of cloud liquid water data, MSc. thesis, McGill University, 69pp.

[9] Brosamlen, G., Lovejoy, S. and Schertzer, D. 1994, Multifractal analysis of cloud liquid water over the range 5m to 330 km: a new test of the unified scaling model. (submitted to J. Atmos. Sci.).

[10] Cahalan, R. F. 1989, Overview of fractal clouds, paper presented at RSRM'87, Advances in Remote Sensing, 371-389, edited by A. Deepak et al., A. Deepak, Hampton, Va.

[11] Cahalan, R. F. 1994, Bounded cascade clouds: albedo and effective thickness, Nonlinear processes in Geophysics, 2/3, 156-167.

[12] Chigirinskaya, Y., Schertzer, D., Lovejoy, S., Lazarev, A. and Ordanovich, A. 1994, Unified multifractal atmospheric dynamics tested in the tropics Part 1: horizontal scaling and self organized criticality, Nonlinear Processes in Geophysics, 2/3, 105-114.

[13] Davis, A., Lovejoy, S., Gabriel, P., Schertzer, D. and Austin, G. L. 1990, Discrete angle radiative transfer. Part III: numerical results on homogeneous and fractal clouds. J. Geophys. Res. 95, 11729-11742.

[14] Davis, A., Lovejoy, S. and Schertzer, D. 1991a, Discrete angle radiative transfer in a multifractal medium, Ed. V. V. Varadan, SPIE, 1558, 37-59.

[15] Davis, A., Lovejoy, S. and Schertzer, D. 1991b, Radiative transfer in multifractal clouds. In Non-linear variability in geophysics: Scaling and Fractals. Kluwer, Schertzer, D. and Lovejoy S. (ed.s), pp. 303-318.

[16] Davis, A., Marshak, A., Wiscombe, W. and Cahalan, R. 1994, Multifractal characterization of nonstationary and intermittency in geophysical fields: observed, rtrieved or simulated, J. Geophys. Res., 99, 8055-8072.

[17] Dremin, I. M., 1994, Fractality and the anomalous dimension of Quantum Chromodynamics, Fractals in the natural and applied sciences, M. M. Novak Ed. 101-108.

[18] Duncan, M. R. 1993, The universal multifractal nature of radar echo fluctuations, PhD. thesis, McGill University, 220pp.

[19] Duncan, M. R., Lovejoy, S. and Schertzer, D. 1994, Multifractals and the radar observer's problem, (submitted to J. Atmos. Sci.)

[20] Duncan, M. R., Lovejoy, S., Fabry, F. and Schertzer, D. 1993, Radar measurement scales and nonuniformity in the rainfield. The 2nd Inter. Symp. on Hydrological Appl. of Weather Radar, Univ. of Hannover, Sept. 7-10th.

[21] Endlich, R. M. and Mancuso, R. L. 1968, Objective analysis of environmental conditions associated with severe thunderstorms and tornadoes. Mon. Wea. Rev. 96, 342-350.

[22] Evans, K. F., 1993, A general solution for stochastic radiative transfer, Geophys. Res. Lett., 20, 19, 2075-2078.

[23] Fan, A. H., 1989, Chaos additif et multiplicatif de Levy. C.R. Acad Sci. Paris I, 308 , 151- 154.

[24] Francis, F., 1993, Multifractal characteristics of sea ice from SAR imagery. 3rd year report, Physics, McGill University.

[25] Gabriel, P., Lovejoy, S., Austin, G. L. and Schertzer, D. 1986, Radiative transfer in extremely variable fractal clouds, 6th conference on atmospheric radiation, 230-234, AMS, Boston.

[26] Gabriel, P., Lovejoy, S., Schertzer, D. and Austin, G. 1988, Multifractal analysis of resolution dependence in satellite imagery. J. Geophys. Res. 15, 1373-1376.

[27] Gabriel, P., Lovejoy, S., Davis, A., Schertzer, D. and Austin, G. L. 1990, Discrete angle radiative transfer. Part II: renormalization approach to scaling clouds. J. Geophys. Res. 95, 11717-11728.

[28] Gaonac'h, H., Lovejoy, S.and Stix, J. 1992, The resolution dependence

of basaltic lava flows and their fractal dimensions. Geophys. Res. Lett. 19, 785-788.

[29] Garrido, P., Lovejoy, S. and Schertzer, D. 1993, Universal multifractals and the large scale structure of the universe, (in preparation).

[30] Hooge, C., 1993, Earthquakes as a space-time multifractal process, MSc thesis, McGill University, 152pp.

[31] Hooge, C., Lovejoy, S., Schertzer, D., Schmitt, F. and Malouin, J. F. 1994, Multifractal phase transitions: the origin of self-organized criticality in earthquakes, Nonlinear Proc. in Geophys. (in press).

[32] Hubert, P., Tessier, Y., Lovejoy, S., Schertzer, D., Ladoy, P., Carbonnel, J. P. and Violette, S. 1993, Multifractals and extreme rainfall events. Geophys. Res. Lett. 20, 931-934.

[33] Kerman, B., 1993, A multifractal equivalent of the Beaufort scale for sea-state. Geophys. Res. Lett., 20, 297-300.

[34] Ladoy, P., Schertzer, D. and Lovejoy, S. 1986, Une étude d'invariance locale-regionale des temperatueres, La Météorologie, 7, 23-34.

[35] Ladoy, P. Schmitt, F., Schertzer, D. and Lovejoy, S. 1993, observations pluviométriques à Nimes, C. R. Acad. des Sciences, 317, II, 775-782.

[36] Larnder, C., Desaulniers-Soucy, N., Lovejoy, S., Schertzer, D., Braun, C. and Lavallée, D. 1992, Universal multifractal characterization, and simulation of speech, Int. J. Bifurcation and Chaos, 2, 715-719.

[37] Lavallée, D. 1991, Multifractal techniques: analysis and simulations of turbulent fields. Ph.D. thesis, McGill University, Montreal, Canada.

[38] Lavallée, D., Lovejoy, S., Schertzer, D. and Ladoy, P. 1993a, Nonlinear variability and landscape topography: analysis and simulation. Fractals in Geography, ed.s L. De Cola and N. Lam, 171-205.

[39] Lavallée, D., Jourdan, D., Gautier, C., and Hooge, C. 1993b, Universal multifractal properties of microwave satellite data. Proc. of Hydrofractals, '93, p. 21-26.

[40] Lazarev, A., Schertzer,D., Lovejoy, S. and Chigirinskaya, Y. 1994, Unified multifractal atmospheric dynamics tested in the tropics: part II, vertical scaling and Generalized Scale Invariance, Nonlinear Processes in Geophysics, 1, 115-123.

[41] Lewis, G. 1993, The Scale Invariant Generator technique and scaling anisotropy in geophysics. MSc. thesis, McGill University (110pp).

[42] Lovejoy, S. 1981, Analysis of rain areas in terms of fractals, 20th conf. on radar meteorology, 476-484, AMS, Boston.

[43] Lovejoy, S. and Schertzer, D. 1986, Scale invariance in climatological temperatures and the spectral plateau. Annales Geophys., 4B, 401-410.

[44] Lovejoy, S. and Schertzer, D. 1986, Scale invariance, symmetries, fractals and stochastic simulations of atmospheric phenomena, Bulletin of the Amer. Meteor. Soc, 67, 21-32.

[45] Lovejoy, S. and Schertzer, D. 1989, Fractal clouds with discrete angle radiative transfer. I.R.S. 88, Eds. C. Lenoble and J. F. Geylyn, Deepak publishing, 99-102.

[46] Lovejoy, S. and Schertzer, D. 1990, Fractals, rain drops and resolution dependence of rain measurements, J. Appl. Meteor., 29, 1167-1170.

[47] Lovejoy, S. and Schertzer, D. 1990a, Multifractals, universality classes, satellite and radar measurements of clouds and rain. J. Geophys. Res., 95, 2021-2034.

[48] Lovejoy, S., Gabriel, P., Davis, A., Schertzer, D., and Austin, G. L. 1990b, Discrete angle J. Geophys. Res., 95, 11699-11715.

[49] Lovejoy, S., Schertzer, D., Silas, P., Tessier, Y. and Lavallée, D. 1993, The unified scaling model of the atmospheric dynamics and systematic analysis of scale invariance in cloud radiances, Annales Geophysicae, 11, 119-127.

[50] Lovejoy, S., Schertzer, D., Hooge, C. and Todeschuk, J. 1994a, Multifractal analysis of aeromagnetic data (in preparation for Geophys. Res. Lett.)

[51] Lovejoy, S., Watson, B., Brosamlen, G. and Schertzer, D., 1994b, A multifractal formalism for scattering statistics in multifractal clouds (prepared for J. Stat. Phys.)

[52] Lovejoy, S., Lavallée, D., Schertzer, D. and Ladoy, P. 1994c, The $l^{\frac{1}{2}}$ law and multifractal topography, submitted to Nonlinear Proc. in Geophys.

[53] Mandelbrot, B. 1967, How long is the coastline of Britain? Statistical self-similarity and fractional dimension. Science, 155, 636-638.

[54] Mandelbrot, B. 1983, The Fractal Geometry of Nature, Freeman, San Francisco.

[55] Meakin, P. 1987, Random walks on multifractal lattices, J. Phys. A, 20, L771-L777.

[56] Meneveau, C. and Sreenevasan, K. R. 1987, Simple multifractal cascade model for fully developed turbulence. Phys. Rev. Lett., 59, 13 , 1424-1427.

[57] Naud, C., Schertzer, D. and Lovejoy, S. 1994, Analysis and simulation of radiative transport in multifractal disordered media, Stochastic models in geosystems, Ed. W. A. Woyczynski, Institute of Mathematics and its Applications (in press).

[58] Nguyen, V. T. V., Pandley, G. R. and Rousselle, J. 1993, Estimation

of missing short-duration rainfalls using data measured at longer time scales. Proc. of the 6th Inter. Conf. on Urban Storm Drainage, September 12-17, 1993, Niagara Falls, Ontario, Canada, Vol. 1, Edited by J. Marsalek, and H. C. Torno, pp. 170-175.

[59] Olsson, J. 1994, Estimation of multifractal parameters for a high-resolution rainfall time series, Nonlinear Processes in Geophysics (submitted).

[60] Parisi, G., and Frisch, U. 1985, A multifractal model of intermittency. Turbulence and predictability in geophysical fluid dynamics and climate dynamics., 84-88, Eds. M. Ghil, R. Benzi, G. Parisi, North-Holland.

[61] Pecknold, S., Lovejoy, S., Schertzer, D., Hooge, C. and Malouin, J. F. 1993, The simulation of universal multifractals. Cellular Automata: Prospects in astrophysical applications, Eds. J. M. Perdang, A. Lejeune, World Scientific, pp. 228-267.

[62] Perrin, J. 1913, Les Atomes, NRF-Gallimard, Paris.

[63] Pflug, K., Lovejoy, S. and Schertzer, D. 1993, Generalized Scale Invariance, differential rotation and cloud texture: analysis and simulation, J. Atmos. Sci., 50, 538-553.

[64] Ratti, S. P., Salvadori, G., Gianini, G., Lovejoy, S. and Schertzer, D. 1994, A Universal multifractal approach to intermittency in high energy physics, Z. Phys. C61, 229-237.

[65] Richardson, L. F. 1961, The problem of contiguity: an appendix of statistics of deadly quarrels. General Systems Yearbook, 6, 139-187.

[66] Salvadori, G., Ratti, S. P., Belli, G., Lovejoy, S. and Schertzer, D. 1994, Multifractal objective analysis of Seveso ground pollution. Toxicol. and Environ. Chem. 43, 63-76.

[67] Saucier, A. 1992, Effective permeability of multifractal porous media, Physica A, 183, 381- 397.

[68] Schertzer D. and Lovejoy, S. 1985a, The dimension and intermittency of atmospheric dynamics, Turbulent Shear flow 4, 7-33, B. Launder ed., Springer.

[69] Schertzer, D. and Lovejoy, S. 1985b, Generalised scale invariance in turbulent phenomena Physico-Chemical Hydrodynamics Journal, 6, 623-635.

[70] Schertzer, D. and Lovejoy, S. 1987, Physically based rain and cloud modelling by anisotropic, multiplicative turbulent cascades. J. Geophys. Res., 92, 9692-9714.

[71] Schertzer, D. and Lovejoy, S. 1989, Nonlinear variability in geophysics: multifractal analysis and simulations. Fractals: their physical origins and properties, Pietronero ed., Plenum Press, New York, 49-79.

[72] Schertzer, D. and Lovejoy, S. 1991a, Scaling, fractals and non-linear variability in geophysics, Kluwer, 318pp.

[73] Schertzer, D. and Lovejoy, S. 1991b, Nonlinear geodynamical variability: multiple singularities, universality and observables. In: Scaling, fractals and non-linear variability in geophysics, D. Schertzer and S. Lovejoy ed.s, Kluwer, 41-82.

[74] Schertzer, D., Lovejoy, S., Lavallée, D. and Schmitt, F. 1991, Universal hard multifractal turbulence, theory and observations. Nonlinear Dynamics of Structures, R. Z. Sagdeev et al. ed.s, World Scientfic, 213-235.

[75] Schertzer, D. and Lovejoy, S. 1992, Hard and soft multifractal processes: Physica A, 185, 187- 194.

[76] Schertzer, D. and Lovejoy, S. 1993, Multifractal generation of self-organized criticality, In: Fractals in the natural and applied sciences, M. M. Novak, ed., Elsevier North-Holland, 325-339.

[77] Schertzer, D., Lovejoy, S. and Lavallée, D. 1993, Generic multifractal phase transitions and self-organized criticality. In: Cellular automata: prospects in astrophysical applications, J. M. Perdang and A. Lejeune, ed.s, World Scientific, pp. 216-227.

[78] Schertzer, D. and Lovejoy, S. 1994a, From scalar cascades to Lie cascades: joint multifractal analysis of rain and cloud processes. In: Space/time Variability and Interdependence for Various Hydrological Processes, R. A. Feddes, ed., Cambridge University Press, in press.

[79] Schertzer, D. and Lovejoy, S. 1994b, Multifractals and turbulence: fundamentals and applications, World Scientific (in press).

[80] Schertzer, D. and Lovejoy, S. 1994c, Standard and advanced multifractal techniques in remote sensing (this volume).

[81] Schmitt, F., Lavallée, D., Schertzer D. and Lovejoy, S. 1992, Empirical determination of universal multifractal exponents in turbulent velocity fields, Phys. Rev. Lett., 68, 305-308.

[82] Schmitt, F., Schertzer, D., Lovejoy, S. and Brunet, Y. 1994, Estimation of universal multifractal indices for atmospheric turbulent velocity fields. Fractals, 3, 568-575.

[83] Schmitt, F., Schertzer, D., Lovejoy, S. and Brunet, Y. 1994, Empirical study of multifractal phase transitions in atmospheric turbulence, Nonlinear Processes in Geophysics, 2/3, 95-104.

[84] Segal, B. 1979, High-intensity rainfall statistics for Canada, no. CRC 1329-E, Ottawa (Ontario), Canada.

[85] Silas, P. K., Lovejoy, S. and Schertzer, D. 1993, Single phase diffusion in multifractal porous rock, Proceedings of Hydrofractals '93, p1-6.

[86] Steinhaus, H. 1954, Length, shape and area. Colloquium Mathematicum, 3, 1-13.

[87] Steinhaus, H. 1962, Mathématiques en instantanés, Paris, Flamarion.

[88] Tessier, Y., Lovejoy, S. and Schertzer, D. 1993a, Universal fractals in rain and clouds: theory and observations, J. Appl. Meteor., 32, 223-250.

[89] Tessier, Y., Lovejoy, S., Schertzer, D., Lavallée, D. and Kerman, B. 1993b, Universal multifractal indices of the ocean surface at far red wavelengths, Geophys. Res. Lett., 20, 1167-1170.

[90] Tessier, Y., Hubert, P., Carbonnel, J. P., Lovejoy, S. and Schertzer, D. 1993c, Phase transitions and universal multifractals in river flows. Proceedings of Hydrofractals '93, A1-A6.

[91] Tessier, Y., Lovejoy, S. and Schertzer, D. 1994, The multifractal global raingauge network: analysis and simulation, (J. Appl. Meteor., in press).

[92] Venig-Meinesz, F. A. 1951, A remarkable feature of the Earth's topography. Proc. K. Ned. Akad. Wet. Ser. B Phys. Sci., 54, 212-228.

[93] Visvanathan, R., Weber, C. and Gibart, P. 1991, The stochastic coherence and the dynamics of global climate models and data. In Non-linear variability in geophysics: Scaling and Fractals. Kluwer, D. Schertzer and S. Lovejoy ed.s, pp. 269-278.

[94] Wilson, J., Lovejoy, S. and Schertzer, D. 1991, Physically based cloud modelling by scaling multiplicative cascade processes. Scaling, fractals and non-linear variability in geophysics, D. Schertzer and S. Lovejoy ed.s, 185-208, Kluwer.